Operational Characteristics of a Plasma Torch for Supersonic Combustion Applications with Simulated Cracked JP-7 Feedstock

Melissa A. Cross

Thesis Submitted to the Faculty of
Virginia Polytechnic Institute and State University
in partial fulfillment of the requirements for the degree of

Master of Science

In

Mechanical Engineering

Dr. Walter F. O'Brien, chair

Dr. Joseph A. Schetz

Dr. Peter S. King

Dr. Scott D. Gallimore

May 7, 2004
Blacksburg, VA

Supersonic plasma torch hydrocarbon

Operational Characteristics of a Plasma Torch for Supersonic Combustion Applications with Simulated Cracked JP-7 Feedstock

By

Melissa Cross

W.F. O'Brien, Chairman

Mechanical Engineering

(ABSTRACT)

Research conducted at Virginia Tech has examined plasma torch operational characteristics using a feedstock gas of mixed hydrocarbons representing a cracked JP-7 surrogate. The tests were part of a program to examine the torch as an igniter and flame-holder for hydrocarbon-fueled scramjet engines. Previous research has shown that the plasma torch has promise as a robust igniter and flame-holder using gaseous fuels such as methane, ethylene and propylene when combined with an aeroramp to assist with the combustion process. The present investigation tested the plasma torch with a feedstock mixture of gaseous hydrocarbons that simulates thermally cracked JP-7 jet fuel. This simulation of a cracked hydrocarbon fuel was studied to lay the foundation for work with liquid hydrocarbon fuel, which is of interest for today's aerospace vehicles. The cracked JP-7 surrogate consists of a 15/25/60 mixture of methane/ethane/ethylene. The research results include torch operational characteristics such as downstream plume temperatures and emission spectroscopy within the combustion plume, as well as the power supplied to the torch over a range of mass flow rates. Filtered photographs of the emissions plume were studied to aid torch plume diagnostics. Other observations made were erosion and alignment of the electrodes, which will help determine the potential lifespan of the torch

using cracked JP-7 fuel. The results show successful operation over a range of powers with simulated cracked JP-7 feedstock flows. Measured spectra, current, and voltage are compared with similar results for other hydrocarbon feedstock gases. The torch operating on the JP-7 surrogate feedstock appears to be a satisfactory device for ignition, flame-holding, and combustion enhancement of cracked hydrocarbons in supersonic combustion.

Acknowledgements

First and foremost, I would like to thank Bill for being there for me. You always seem to find the lighter side of things even where the end of the tunnel was no where to be seen. You were there when I needed help running tests, when I needed someone to proofread, and when I needed to take my mind off of the work for a while.

I would like to thank my family who kept me motivated on a personal level. The amount of support from you to continue and complete my education has not been unnoticed.

I would also like to thank my committee, for without them, I would be truly lost and would not know where to begin my research. I can not even begin to describe the amount of guidance and expertise you have given me. The amount of knowledge amongst you is truly amazing.

The fine people at NASA Langley are deeply appreciated for their support, encouragement, and beliefs in this work.

A special thanks goes to Darius for working through this project with me. I know I would not have been able to finish this work without your help and still be sane. Joe, Cody, Ari, Matt, and Tiffany are due thanks for their ideas and support…and for staying away from equipment that is in working condition, you know who you are.

Steve, you are awesome. Without your help, I don't know how long it would have taken to figure out how to wire up all of our equipment and decipher all of the LabView code. The AOE and ME machine shops are due thanks as well. Without your help, none of this would have happened since we wouldn't have anything to test with.

Finally, the turbolabbers: Pete, Joe, Kevin, Mano, Mac, John, Matt, Matthew, Rob, Hoon, Kevin, Katie, Tiffany, and Darius. You made life in front of a computer, in a basement, with no windows, fun…is that possible? The extended families of turbolabbers were great as well: Jennifer, Ian, Lorette, Mrs. O'Brien, Michelle, and Micah. Your dinners and treats as well as the entertainment of the little ones are always welcome in my book.

Table of Contents

List of Figures

List of Tables

Nomenclature

Symbols

A	Concentration of specie “A”
B	Concentration of specie “B”
d	Diameter
E_A	Activation energy
I	Intensity
k_B	Boltzmann constant
λ	Wavelength
μ	Reduced mass
M	Mach number
N_{AV}	Avagadro’s number
p	Steric factor
P	Pressure
R_u	Universal gas constant
σ_{AB}	Collision cross section
t	Time
T	Temperature
TTR	Total temperature ratio
W	Watts
Y	Spanwise coordinate
Z	Vertical coordinate

Subscripts

∞	Freestream
eff	Effective
o or t	Total

Chapter 1

History and Development

Early aircraft were propelled by gasoline-powered engines driving a propeller. Many years later came the turbojet engine was developed which utilizes an internal compressor and turbine in several stages to produce thrust. This is still a very common engine that can be found on many commercial and military aircraft. This type of engine can only produce enough thrust to power an aircraft from subsonic speeds up to approximately Mach 3. With the desire to go faster another engine is needed, leading to the development of the ramjet engine. The ramjet engine has limitations due to losses from the deceleration of airflow required for stable combustion, so another engine, the supersonic combustion ramjet (scramjet) engine, was developed to allow for even faster flight. Since the ramjet and scramjet have many similarities, a discussion of each engine follows.

1.1. The Ramjet Engine

The ramjet, developed from the early 1900s through the 1960s, is a fairly simple engine since it does not require the use of turbomachinery. Supersonic inlet air is diffused to subsonic speeds by means of geometry variations within the duct. The air, moving at velocities comparable to what a turbojet engine would experience, then passes through a combustion region and is forced out of the engine through a nozzle. A simple schematic showing the inlet, diffuser, burner and nozzle of a ramjet engine can be seen in Figure 1.1 with air flowing from left to right. One limitation of a ramjet engine is a maximum flight velocity of about Mach 6 due to the losses incurred by decelerating the air flow. Another limitation would be the inability to take off like a conventional aircraft since it cannot produce thrust at very low speeds. A ramjet powered aircraft needs an alternate method

of propulsion to accelerate the aircraft to ramjet design conditions. As fast as a ramjet-propelled vehicle can be, today's researchers desire an engine that can propel an aircraft much faster than Mach 6, which lead to the development of the scramjet engine.

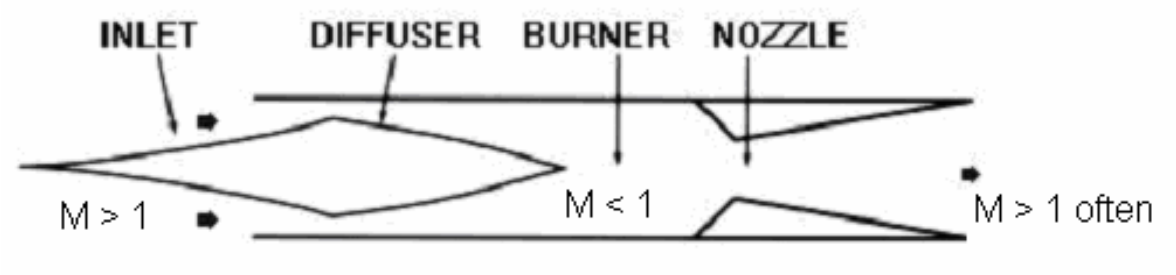

Figure 1.1: A Ramjet Engine [http://www.aviation-history.com]

1.2. The Scramjet Engine

Scramjet engines were first developed in the 1950s and 1960s at Johns Hopkins University and NASA research centers [Waltrup 1987, Waltrup et al. 1976 and Andrews et al. 2001] and are very similar to a ramjet engine with the exception that the air flow through the engine is now entirely supersonic, which allows the engine (and the aircraft attached to it) to travel at speeds greater than Mach 6. This engine can be more efficient than a ramjet engine at these higher Mach numbers since the air flow does not have to slow down to subsonic speeds in the combustion chamber, therefore avoiding diffusion losses. However, when the internal flow of air exceeds Mach 1, the combustor flame can not sustain itself without assistance. In many cases, a pyrophoric additive is introduced in the combustion chamber to aid the combustion process. A simple schematic of a scramjet engine showing the inlet, burner and nozzle can be seen in Figure 1.2 with air flowing from left to right.

In the beginning of scramjet development, there were very few materials that could withstand the extreme temperatures present within the combustion region of a scramjet engine, making the engine impractical during those early years. With today's technologies and materials, scramjet engines are being considered again as a possible

source of thrust for aircraft traveling greater than Mach 6. Many important hypersonic programs over the years contributed to the development of this advanced engine.

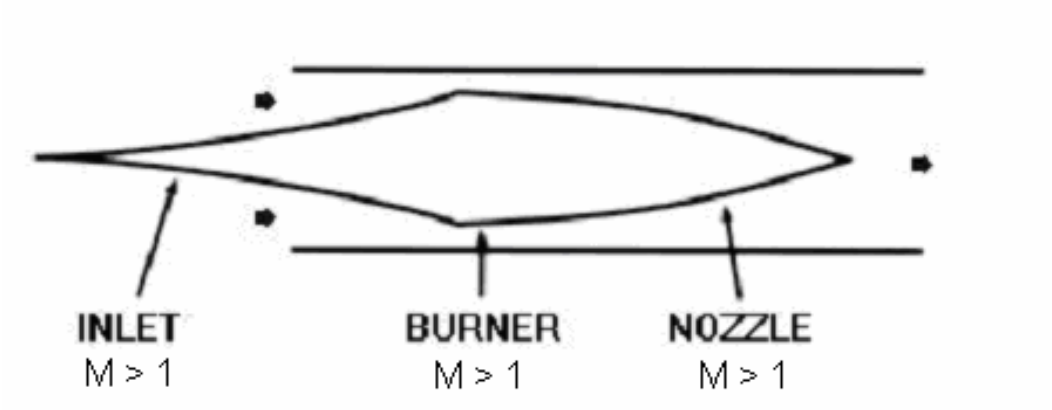

Figure 1.2: A Scramjet Engine [http://www.aviation-history.com]

1.3. The Dual Combustion Ramjet Engine

One interesting engine that came about from the ramjet and the scramjet testing in the 1970s is the Dual Combustor Ramjet (DCR) which was researched mainly at the Johns Hopkins University Applied Physics Laboratory [Curran 2001]. The DCR contains all the features of a scramjet except a small fraction of the intake air is diverted into a subsonic combustion region where liquid hydrocarbon fuel is injected and allows for a near-stoichiometric flame to be maintained. A schematic of the DCR can be seen in Figure 1.3 [Waltrup 1987]. This idea is to allow the use of heavy hydrocarbon fuels without requiring fuel preconditioning, reactive fuel additives or reactive pilots in the combustion process [Waltrup et al. 1996]. A major disadvantage to this concept is the large volume and therefore excess weight from the use of a subsonic gas generator. While not a necessity in subsonic environments, the concept of using a pilot flame to aid combustion has been developed in supersonic combustion by means of a plasma torch, among others, and is the focus of this thesis.

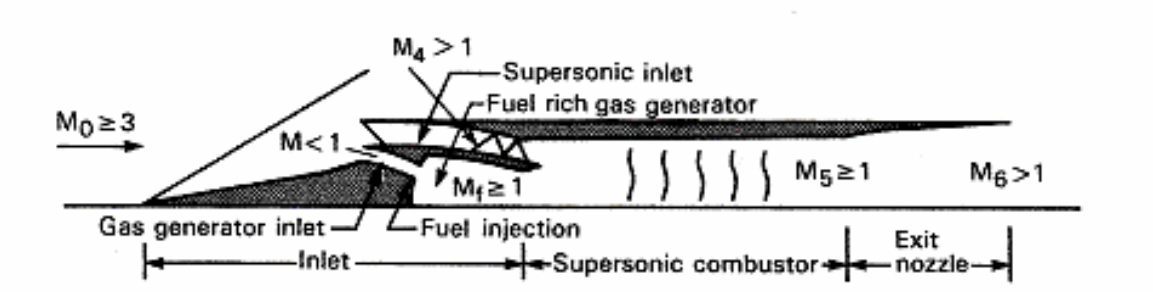

Figure 1.3: The Dual Combustor Ramjet Engine [Waltrup 1987]

1.4. Scramjet Development Programs

The first widely recognized researcher in scramjet technology development was Dr. A. Ferri. He had developed an early scramjet engine and conducted free-jet tests in the GASL Combustion-Heated High-Enthalpy Blow-Down Tunnel in 1963 [Andrews et al. 2001]. He had also verified steady combustion without strong shocks in a Mach 3 supersonic environment [Ferri 1959 and Ferri et al. 1964]. The U.S. Navy has made many contributions to the development of the scramjet engine including demonstrating combustion in a Mach 5 air stream for the first time shortly after Ferri demonstrated Mach 3 combustion [Waltrup et al. 1996]. Even though the U.S. Navy made many significant contributions, the National Aeronautics and Space Administration (NASA) and the U.S. Air Force (USAF) have worked individually and cooperatively on several scramjet-related projects throughout the years.

One of the joint NASA/USAF projects that created an abundance of ground test data for scramjet technologies was the National AeroSpace Plane (NASP), which can be seen in Figure 1.4. NASA Langley had constructed state-of-the-art scramjet test facilities in the 1970s, but in the 1980s, these facilities became the main test beds for the program with the start of the NASP program [Andrews et al. 1985, Andrews 1987, Guy et al. 1981, Thomas et al. 1982, Rock et al. 1991 and Williams 1986]. This program was initiated to develop a single stage to orbit flight research vehicle. Not only did the project result in major breakthroughs in the development of Computational Fluid Dynamics (CFD) codes, it is also one of the more important projects involved in the development of hypersonic

flight, specifically the scramjet engine because of the amounts of data collected during this time. Before the NASP test vehicle had a chance to fly, the program was canceled. However, enough data about scramjet engines were collected which allowed researchers to continue investigating hypersonic propulsion.

The U.S. Air Force began its scramjet research by conducting tests of scramjet engines running on hydrogen. Based on a change in focus from large scramjet vehicles to smaller missile systems, the Air Force began looking at scramjet engines running on simple gaseous hydrocarbon fuels with a high density impulse such as methane and ethylene. Early in their hydrocarbon testing, the Air Force modified existing hydrogen scramjets by extending the combustion chamber to allow for the longer ignition delay time of the hydrocarbon fuels. Early designs did not provide a successful hydrocarbon scramjet engine [Waltrup 1987, Waltrup et al. 1976 and Curran 2001]. However, with technology progressing steadily since the conception of the scramjet engine in the 1950s and 1960s, unsuccessful attempts in these early development stages contain useful information to contribute to promising results in current investigations including the addition of a pilot system that allowed the modified scramjet engine to operate on hydrocarbon fuels.

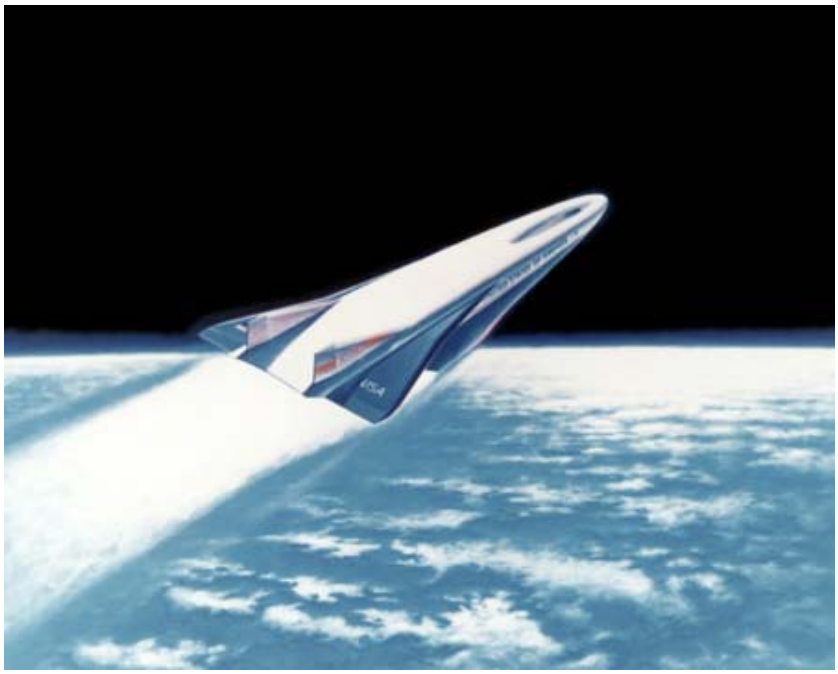

Figure 1.4: The National AeroSpace Plane concept drawing [http://nix.nasa.gov]

One of the more recent programs involving scramjet technologies is the Hyper-X Program which is a joint NASA Langley Research Center/NASA Dryden Flight Research Center project. It is a project aimed at implementing the laboratory technologies developed over the years into an actual flight test bed. The first vehicle under this project is the airframe-integrated gaseous hydrogen scramjet-powered X-43A and is designed to fly at Mach 7. The first test flight of the X-43A was lost due to a malfunction of the launch vehicle. The X-43A was not canceled due to this unfortunate mishap. A successful flight on March 27, 2004 provided much needed encouragement for future developments in hypersonic research, such as how to cool the vehicle for flights lasting longer than the recent ten second flight as well as how to balance the operational craft without the addition of an 800 pound counterweight that constitutes 29% of the gross weight [Dornheim 2004].

The second vehicle in the Hyper-X Program was the X-43C which was a NASA/USAF/industry collaboration. Compared to the X-43A, the X-43C vehicle was designed to be volumetrically more efficient in order to carry the different fuel; the X-43C was designed to use a hydrocarbon based fuel. The engine of the X-43C was wider than the X-43A to provide a greater air capture and higher thrust for robust acceleration. The X-43C would have had three flights where it was to accelerate from Mach 5 to Mach 7 under its own power and autonomous control. Each flight vehicle would have been powered by a hydrocarbon-fueled, fuel-cooled, dual-mode, airframe-integrated scramjet engine system developed under the HyTech Program of the USAF. Between Mach 4 and Mach 8, liquid hydrocarbon fuels are preferred over hydrogen based fuels due to the higher density (and corresponding fuel tank volume) and safe handling considerations of the hydrocarbon fuels. The use of hydrocarbon fuels allows for a much longer flight than hydrogen permits. As a comparison, Figure 1.5 shows the air specific impulse (I_{sp}) versus Mach number for different engines operating on hydrocarbon fuels and hydrogen fuels. The specific impulse indicates the amount of pounds of thrust produced per pound mass of fuel and oxidizer injected into the engine per second. The first flight in the X-

43C program was scheduled for 2007 [Moses 2003] but due to recent events the X-43C program has been canceled.

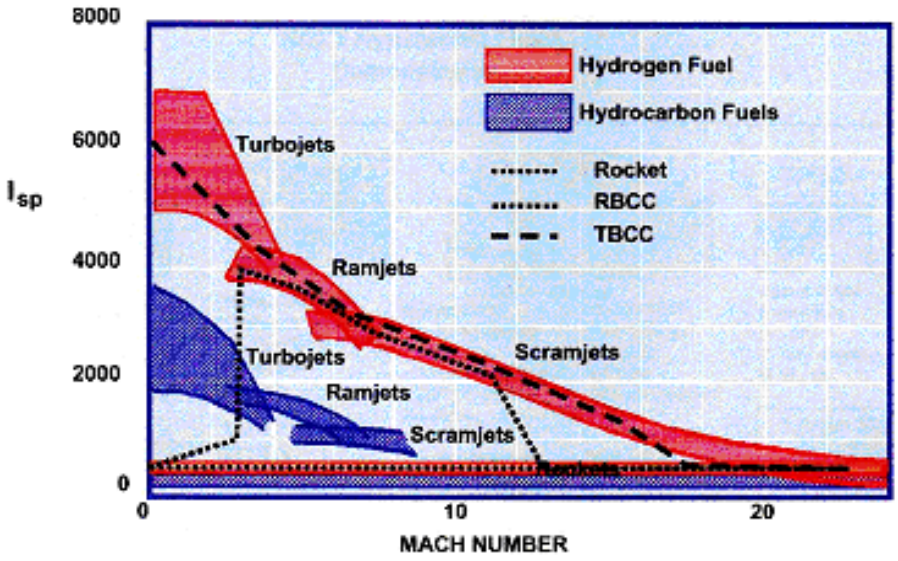

Figure 1.5: Performance Levels of Various Engines [Moses 2003]

1.5. Benefits of a Plasma Torch

As stated previously, combining the fuel with pyrophoric additives is a common method to assist the combustion process in a ramjet or a scramjet engine. One frequently used pyrophoric additive is silane (SiH_4) which is a substance that requires special handling as are any pyrophoric substances due to their ability to spontaneously ignite when exposed to air. Since these particular substances require extra attention, if a device such as a plasma torch can prove to be just as beneficial and require less maintenance, the plasma torch could prove to be a better combustion aid than the pyrophoric substance. One way to gauge the success of an alternative method is to compare the ignition delay time of silane to the products of the alternative method. A diagram showing ignition delay times calculated for hydrogen using a finite-rate chemical kinetics code can be seen in Figure 1.6 [Wagner et al. 1989]. These results show that 0.1% of monatomic hydrogen is as effective as 20% silane in reducing ignition delay times at lower temperatures. It should

be noted that the temperature on the horizontal axis is decreasing from left to right. If the alternative method to be used can produce an appropriate amount of hydrogen under the conditions shown in Figure 1.6, then that alternative method would be an equivalent replacement of silane, the combustion aid that was scheduled to be used on the X-43C flight demonstrator.

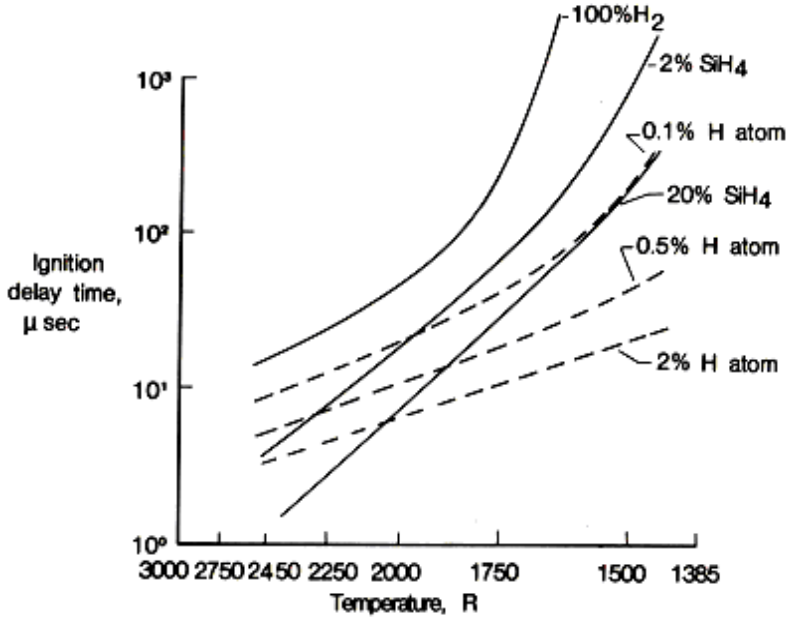

Figure 1.6: Ignition Delay Times of Hydrogen vs. Silane [Wagner et al. 1989]

One alternative method to consider is a plasma torch fed by a hydrocarbon fuel [Gallimore et al. 2002, Jacobsen et al. 2003, Kitagawa et al. 2003, Kuo et al. 2003, Shuzenji 2001]. Hydrocarbon fuels have been studied over the years and have been determined to produce many hydrogen radicals when given a minimal amount of energy from a plasma torch. A study of methane and ethylene plasmas showed that as the chain length of the hydrocarbon feedstock increases, the atomic hydrogen density within the plasma jet also increases [Gallimore et al. 2002]. Many single hydrocarbon fuels have been studied including methane, ethane and ethylene. The research presented here will focus on a mixture of several hydrocarbon chains that simulate thermally cracked JP-7. This mixture will be discussed in more detail in a later section. Thermally cracked JP-7 is an important fuel to consider since vehicles traveling faster than Mach 6.5 will likely

require an endothermic liquid hydrocarbon, such as JP-7, as a structural coolant [Waltrup 2001]. Since there will be a large energy transfer from the structure to the liquid JP-7 during the cooling process, the liquid will endothermically crack before entering the combustion chamber and igniting.

JP-7 fuel is an easily accessible fuel found on some aircraft in the U.S. military and experimental aircraft including the X-43C. The X-43C vehicle will carry this hydrocarbon fuel which has a greater density than hydrogen fuel and allows a greater fuel weight to be carried in the same tank capacity which in turn will help keep the X-43C relatively small. An image of the X-43C Flight Demonstrator can be seen in Figure 1.7. Even though NASA has several vehicles running on hydrogen fuel and continues to develop hydrogen-fueled vehicles, JP-7 fuel is more logistically supportable within the U.S. military than hydrogen fuels [Kelly 2002]. As a matter of fact, it is the X-43C program that generated the interest in how a plasma torch would operate while running on a feedstock of JP-7, and if this combustion process will provides and alternative to silane.

Figure 1.7: The X-43C Flight Demonstrator [http://nix.nasa.gov]

1.6. Development of Plasma Torches

Although the idea of combining electrical power to a flame by means of an arc discharge was conceived as early as 1924 by Southgate, others such as Karlovitz and Weinberg et al. were some of the first to actually implement the idea [Harrison et al. 1971]. Weinberg had discussed that using this device to generate radicals at high temperatures for flame stabilization was thermodynamically and economically unsound in large quantities, but by heating a small portion of the gas to a very high temperature with a small electrical contribution may result in success [Wienberg 1968 and Lawton et al. 1969]. These discussions led to experiments conducted in 1971 using a magnetically rotated plasma jet that stabilized methane flames in high speed flows. These experiments showed that with an addition of 10% electrical power an increase of 700% combustor volumetric flowrate was obtained, however the flame temperature only increased by 116 K. Similar results were obtained when other feedstocks containing hydrogen and oxygen were used. Tests were also conducted using argon as the feedstock gas, but the results seen with hydrogen and oxygen were far superior, leading to the conclusion that combustion enhancement was due to the presence of combustion enhancing radicals as opposed to the addition of electrical or thermal energy [Harrison et al. 1971]. Later experiments conducted by Weinberg et al. complemented these early tests and only strengthened the conclusion that a small amount of electrical power supplied to a small volume of gas containing combustion enhancing radicals could be used to enhance combustion and to stabilize a flame [Weinberg et al. 1978 and Orrin et al. 1981].

The most effective combustion-enhancing radical has been argued to be nitrogen or oxygen, but Weinberg has noted that the effectiveness of the feedstock is determined by the application for which it is being used. Kimura et al. [1981] conducted some of the earliest work to determine how radical addition affected combustion. Their work focused on nitrogen and oxygen where the oxygen was found to ignite a wider range of fuel-air mixtures and reduced the ignition delay time more than the nitrogen. In 1999, Takita et al. [Takita et al. 1999] found that oxygen and nitrogen had comparable results, but in 1993, a study by Masuya et al. [Masuya et al. 1993] found nitrogen to be more effective

than oxygen. Work conducted by Kimura et al. in 1981 [Kimura et al. 1981], found hydrogen to be most effective even though most research has suggested it is not as effective as nitrogen or oxygen can be. In the way of molecules, the hydroxyl molecule (OH) has been shown to reduce ignition delay time by at least 10 times [Pellett 2002]. The hydroxyl molecule is formed by chain branching reactions containing the hydrogen and oxygen radicals such as the two chain branching reactions

$$H + O_2 \leftrightarrow OH + O \quad (1)$$

$$O + H_2 \leftrightarrow OH + H. \quad (2)$$

The dissociation of air includes the reactions

$$O_2 \leftrightarrow 2O \quad (3)$$

$$N_2 \leftrightarrow 2N \quad (4)$$

which occur in equilibrium. For further details on the dissociation of air as well as a complete theory of electric arcs and plasmas, refer to Cobine [1958]. As one can see, there are many results and opinions on which radicals could be the most effective for enhancing combustion. Overall, nitrogen, oxygen and hydrogen radicals have always been thought to be the three most important for combustion enhancement.

The role of a plasma torch is to locally increase the amount of radicals available for combustion reaction and therefore increase the reaction rate. The rate of reaction is a function of collision geometry, temperature and concentration of reactants involved as shown in the Arrhenius kinetic equation

$$-\frac{d[A]}{dt} = pN_{AV}\sigma_{AB}^2\left[\frac{8\pi k_B T}{\mu}\right]^{1/2} \exp\left[\frac{-E_A}{R_u T}\right][A][B]. \quad (5)$$

In the current work, a hydrocarbon-based fuel is used, therefore hydrogen radicals are an expected result. These hydrogen radicals would indirectly produce oxygen radicals by the chain branching reaction shown in Equation 1, where O, OH and H would continue to react with fuel molecules and other chain branching reactions.

Barbi conducted tests based on the knowledge that hydrogen radicals would be beneficial to combustion enhancement [Barbi et al. 1986]. He ran a plasma torch on pure hydrogen to determine if an uncooled, low-power plasma torch would operate and found that a pure

hydrogen feedstock produced unstable operating conditions. He then attempted the same tests with a mixture of hydrogen and argon feedstock which proved to be a more stable feedstock fuel [Barbi et al. 1989]. This work shows that even though a single radical may benefit combustion, a mixture containing that radical may be the better solution by improving the operational stability of a plasma torch. Since hydrocarbon fuels are plentiful in the aerospace industry, it would only be suitable to study the operation of a plasma torch running on a hydrocarbon fuel based on the knowledge that hydrogen radicals are beneficial to combustion enhancement.

The promising results of Weinberg et al. encouraged Kimura et al. to take their work a step further by introducing a plasma torch into a supersonic environment [Kimura et al. 1981]. They used hydrogen plasmas in various Mach numbers, greater than 2, and very low static temperatures of both the air stream and hydrogen fuel. By supplying electrical energy of about 2% of the total chemical energy throughput, a 68% increase in the area occupied by the flame at a predetermined downstream distance of the plasma jet was reported. They also found that the location of the plasma jet with respect to fuel injectors was critical. When the plasma torch was located upstream of the fuel injectors, reactions between the plasma plume and injected fuel were minimal. When the plasma torch was placed downstream of the injectors, the energy from the plasma torch was transferred to the dissociation of the fuel molecules before sufficiently being mixed with the air.

Warris and Weinberg had also demonstrated that plasma torches could broaden the flammability limits for combustors exposed to high speed flows. They found that as long as a hydrocarbon was in the fuel mixture, there will always be some flame luminosity, even if there is very little hydrocarbon present, unlike a conventional spark ignition system that requires a fuel-air mixture within certain limits. [Warris et al. 1984]

In 1984, Northam investigated whether or not a plasma torch would be a suitable replacement for silane, a pyrophoric substance [Northam et al. 1984]. As stated previously, these pyrophoric substances require their own storage and injection systems onboard a vehicle which introduces unwanted weight and can be dangerous if not

handled properly. They found that during unconfined supersonic test conditions, a plasma torch was a suitable igniter and flameholder since hydrogen and hydrocarbon fuels could be stabilized by the torch and would blow off when the torch was extinguished. They also confirmed work done by Kimura et al. that the location of the torch with respect to the fuel injectors is critical when trying to obtain the best combustion. [Northam et al. 1984]

Gallimore and Jacobsen worked on determining the operating characteristics of an integrated fuel injector and plasma torch. They implemented a fuel injector called an aeroramp that contained two rows of two holes spaced evenly apart. Each row of holes was angled downstream and toed-in to create additional vorticity and to enhance mixing. An image of the experimental set up of the aeroramp and plasma torch can be seen in Figure 1.8. The aeroramp used in their work displayed similar mixing results to a physical ramp injector without protruding into the cross stream airflow since the aeroramp was a flush wall injector [Jacobsen et al. 2001 and Gallimore et al. 2003]. With this aeroramp, they injected ethylene into the cross stream airflow into the plume of a plasma torch located downstream. The plasma torch was operated on feedstocks such as nitrogen and methane. They determined that the torch feedstock did not change the penetration height of the plume when the torch was operated with the aeroramp in Mach 2.4 airflows but the mass flowrate through the aeroramp had a significant influence on it [Gallimore et al. 2001]. Through this work, they also determined that by increasing the torch power, the emission intensity of the downstream products increased exponentially for both methane and nitrogen torch feedstocks, which is indicative of greater plasma jet reactivity and influence on the surrounding flowfield [Gallimore et al. 2003].

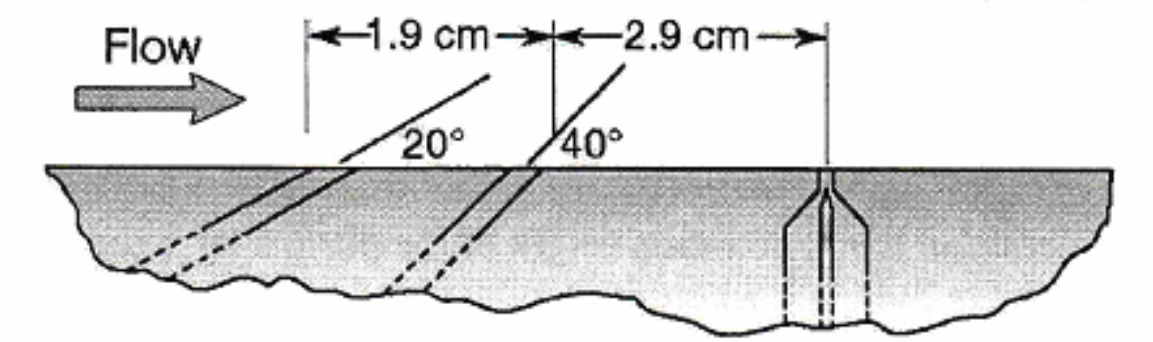

Figure 1.8: Gallimore/Jacobsen Experimental Set-Up of the Aeroramp and Plasma Torch [Gallimore 2001]

The current work is the next step needed to determine how a plasma torch will operate while running on a more complex hydrocarbon fuel. First, the plasma torch was operated with a gaseous surrogate of cracked JP-7 fuel to be able to determine the operating characteristics of the torch. Once the first phase of the work is completed, a liquid surrogate of JP-7 will be used as the torch feedstock which will provide many challenges since the torch being used has only operated on gaseous feedstocks thus far. Once a liquid torch has proven itself, the torch will then be integrated with the aeroramp used in Gallimore's and Jacobsen's work to determine if the same synergistic effects between the plasma torch and the aeroramp hold true when a heavier hydrocarbon fuel is used as the plasma torch feedstock.

Chapter 2

Current Plasma Torch Design and Set-Up

A plasma torch provides a source of energy with an abundance of excited and ionized species. It accomplishes this by passing a feedstock gas through an electrical arc, dissociating the feedstock into a combination of electrons, ions and neutral particles. Plasma torches have been proven to enhance combustion and have been used as flame holding devices in such environments as supersonic combustion chambers. There is a balance between the required power and available space for a power supply onboard a hypersonic vehicle. Also, the feedstock and flowrate of the feedstock may affect the power requirements. Therefore, if a sufficient combination of feedstock gas, range of flow rate and range of power setting can be determined, the supersonic applications can be greatly improved upon.

2.1. The Plasma Torch

The plasma torch used in this research, shown in Figure 2.1, is an uncooled, choked plasma torch modified by Gallimore [2001] and Jacobsen [2001], and originally developed by Phoenix Solutions Co.; it is also known as the Virginia Tech Plasma Torch, 3rd Generation or VTPT-3. This torch incorporates features from previous Virginia Tech designs as well as new features to allow for easy assembly and to allow for stable torch operation. A description of other Virginia Tech plasma torch designs can be found in Appendix A. During this research, the plasma torch was operated at various power settings between 3000 W and 4000 W and was operated solely on the gaseous JP-7 surrogate feedstock.

The plasma torch has two main sections, a negative section and a positive section. The body insulator, labeled as I in Figure 2.1, separates the two sections of the torch. The negative section consists of the cathode (C), the micrometer drive (D) and the cathode bracket (E). The positive section of the plasma torch consists of the anode (A) and the torch body (B). Other important components shown in the diagram are the flow swirler (F), an insulator rod (G), seals (J) and the feedstock line (K). Not shown in Figure 2.1 are the bolts and insulator jackets that hold the torch together which are threaded into part B and a pressure tap to measure the torch chamber pressure.

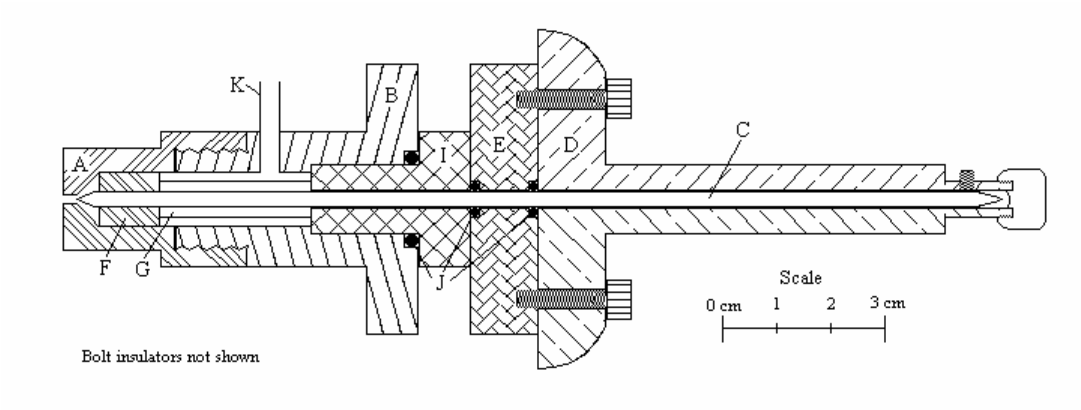

Figure 2.1: Section Drawing of the Current Plasma Torch [Gallimore 2001]

2.2. The Electrodes

The cathode and anode are the only two pieces of the torch that need to be replaced periodically. An electric arc makes a connection with the tip of the cathode and the exit throat of the anode similar to the diagram shown in Figure 2.2. This arc can cause erosion on each electrode after an extended period of time. An image showing the cathode and anode can be seen in Figure 2.3. Electrode life studies have been conducted by Gallimore [2001] on which materials are best suited for the anode for different feedstock gases. It was found that for hydrocarbon based feedstock gases a molybdenum anode was the best material to use based on torch performance, anode erosion rates, and ease of machineability. The internal geometry of the anode included a 1.575 mm

diameter, 2.54 mm long throat. The anode threaded directly to the torch body with a thin layer of Never-Seez® applied to the threads to prevent any fuel leaks. The cathode material was 2% thoriated tungsten, a common welder cathode material. It was a 0.125 inch diameter rod with the ends machined to a 20° half-angle cone. The cathode was attached to the torch by means of a set screw at the end of the micrometer drive. The micrometer drive was turned until the two electrodes made electrical contact then the cathode was backed out until the electrical contact was broken. The cathode was then turned out an additional 0.178 mm to set the gap.

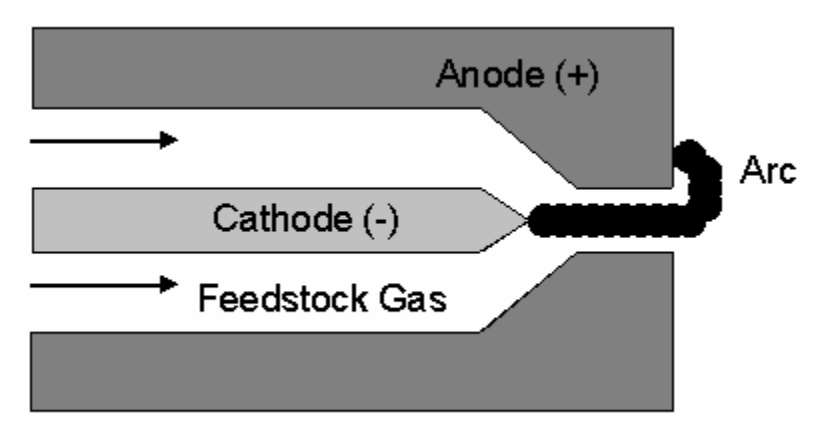

Figure 2.2: Schematic of Torch Electrodes and Arc Attachment Point

Some alignment issues arose from the cathode attachment point being at the base of the micrometer drive. When the torch was developed, care was taken to include guides along the length of the torch to assist with the alignment of the cathode. It is important that the cathode be perfectly centered with the center of the throat of the anode in order for the arc to strike in a rotating pattern with aid from the flow swirler. If the electrodes were not aligned properly, then anode erosion was severe and concentrated in the location of the anode closest to the cathode tip. For all tests conducted, care was taken to assure that the electrodes were aligned to prevent the life of the electrodes from being cut short.

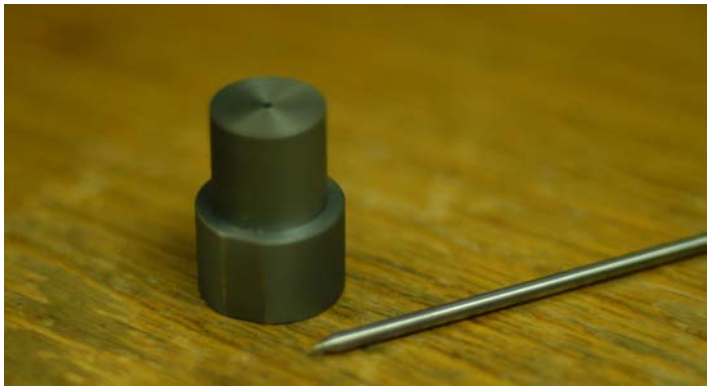

Figure 2.3: Molybdenum Anode (left) and 2% Thoriated Tungsten Cathode (right)

2.3. The Micrometer Drive

The micrometer drive used was a 440 Starrett® depth micrometer (Figure 2.4) which allowed for very accurate readings and simplified gap adjustments. The off-the-shelf depth micrometer had to be modified to be attached to the plasma torch. Two ¼ inch Allen-head screws were used to attach the micrometer to the cathode bracket and can be seen in Figure 2.1. A set screw through the micrometer drive was used to hold the cathode in place and to allow for the fine adjustments when the gap was being set.

Figure 2.4: The Micrometer Drive

2.4. The Torch Body

The torch body, seen in Figure 2.5, was machined from stainless steel to provide a sturdy, corrosion resistant body to hold the torch together. Stainless steel tubes were welded to the body to provide an input for the feedstock gas (K) and for a pressure tap. Never-Seez® nickel lubricant was spread on the threads between the torch body and the anode to prevent gas leaks. On the other end of the torch body, a rubber O-ring was placed around the cathode between the body and micrometer drive to prevent gas leaks through the back end.

Figure 2.5: The Torch Body

2.5. The Flow Swirler and Insulator Rod

The flow swirler used in this work was made from boron nitride, a very brittle but heat resistant material. Three 45° channels cut into the swirler induced vorticity to the torch chamber flow, which caused the arc to rotate about the anode exit. Concerned that choking should only occur at the anode constrictor area, the flow swirler channels were designed to have four times the area than the anode constrictor. The Teflon® insulator

rod acted as a spacer to keep the flow swirler in the area of the anode closest to the exit throat. This allowed the feedstock gas to completely pass through the channels of the flow swirler, as opposed to around the flow swirler in the larger chamber of the torch body. The insulator rod also acted as a cushioning device in case the anode was screwed on too tightly. An image of the flow swirler and insulator rod can be seen in Figure 2.6.

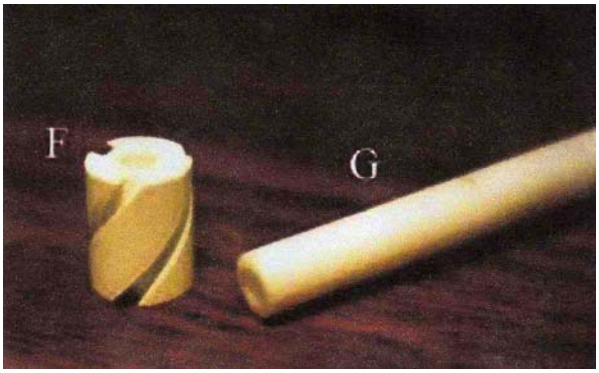

Figure 2.6: The Flow Swirler and Insulator Rod [Gallimore 2001]

2.6. Insulators and Seals

All of the insulators used in the plasma torch were machined out of Teflon® and can be seen in Figure 2.7 [Gallimore 2001]. The insulators were used to keep the positive side of the torch separated from the negative section to prevent shorting of the torch electrical circuit. The bolt insulators (H) acted as isolating jackets since the bolts passed by both positive and negative sections of the torch. Figure 2.7 shows one of the bolt isolators fitted around an Allen-head bolt. The body insulator (I) separated the torch body and the micrometer bracket in a similar fashion. Several O-ring seals (J) were placed around the cathode at different locations of the torch to seal additional leak paths. These are also shown in Figure 2.7. The locations can be seen in Figure 2.1 designated as J. Never-Seez® was also used on the threading of the anode to prevent any feedstock gas leaks.

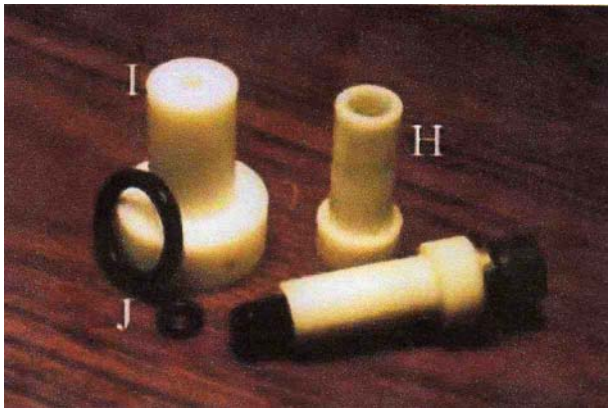

Figure 2.7: Isolators and Seals (H: Bolt Isolator, I: Body Isolator, J: O-Rings) [Gallimore 2001]

2.7. The Surrogate Feedstock Gas

For some hypersonic air breathing vehicle designs being considered by the United States, liquid fuel is routed through the leading edge of the aircraft as a cooling mechanism thereby adding energy to the fuel. For hypersonic flight conditions, the fuel is imparted with such intense heat load that it begins to thermally degrade or "crack." Since the fuel on current vehicles occurs in this cracked state, it was deemed necessary to see how cracked fuel would react when used as the feedstock in a plasma torch. The feedstock used in this work was a mixture of hydrocarbon gases that simulate the products of thermal degradation of advanced endothermic jet fuels developed for high speed flight, specifically thermally cracked JP-7. The mixture consisted of (by volume) 15 % methane, 25 % ethane, and 60 % ethylene [Zelina et al. 1994 and personal conversations with Zelina 2002]. This research did not include the study of pre-heating the torch feedstock, therefore an all-gaseous surrogate recipe was required in order to simulate the cracked state of the fuel. The surrogate recipe chosen contained all gaseous components at room temperature.

Chapter 3

Motivation and Goals

Plasma torches have been deemed an excellent ignition enhancement tool for high speed flows for quite some time. Most of the tests that support this conclusion include plasma torches which operated on feedstocks such as nitrogen, oxygen, argon, hydrogen, methane, ethylene, and other single hydrocarbon gases. Since JP-7 is a possible fuel of choice for future hypersonic vehicles, this work will consider torch operation with a JP-7 surrogate feedstock.

The goals associated with this work involve the following:

1. Determine if the plasma torch is able to operate in a supersonic environment on a surrogate mixture which simulates cracked JP-7.
2. Characterize changes in torch operation with variations in power and flow rate.
3. Study the presence of excited species in the area of reaction by both spectroscopy and filtered photography.
4. Compare surrogate results to methane and ethylene results from previous work.

This work will contribute to the fundamental understanding of the operation of a plasma torch as an ignition enhancer in a supersonic environment. The results of this work will assist with the development of a more efficient igniter which will be beneficial to hypersonic combustion developments.

Chapter 4

Experimental Set-Up and Procedures

All testing for this study was conducted at Virginia Tech in a quiescent test cell and in the Virginia Tech blow-down, unheated supersonic wind tunnel. This chapter describes the equipment and experimental procedures used to collect the data presented in this thesis. The equipment descriptions are presented first, followed by the experimental procedures. A schematic (Figure 4.9) at the end of Section 4.1 shows how the lab equipment was connected to allow for complete data collection during a single run.

4.1. Lab Equipment

The equipment being presented is sorted into the groups that each piece belongs to, such as the quiescent test cell, the wind tunnel, power system, flow measurement, and data acquisition system.

4.1.1. Quiescent Test Cell

The quiescent test cell was used to determine if the plasma torch would ignite under certain power levels and flow rates without the disturbances of a crossflow. The quiescent test cell consisted of several components. An optical table was used to mount the plasma torch and the spectrometer scope. Having both the torch and the spectrometer mounted directly to the optical table allowed the entire assembly to be moved without disturbing the alignment of the two pieces of equipment. The optical table, once set up, could be slid into position into a 25-cm OD X 0.953-cm thick steel pipe located outside of the building with access through a window covered by a 1.25 cm thick piece of Lexan®. The steel pipe was also covered by a sheet of aluminum and a large piece of

fire resistant fabric to shield the test area from precipitation as well any stray light that would interfere with spectrometer readings. The Lexan® was used to prevent unexpected projectiles from entering the test area where the majority of the data acquisition equipment was being held. Small holes were cut into the Lexan® for optical access to enable a camera to take unobstructed images. A photograph of the quiescent test cell can be seen in Figure 4.1.

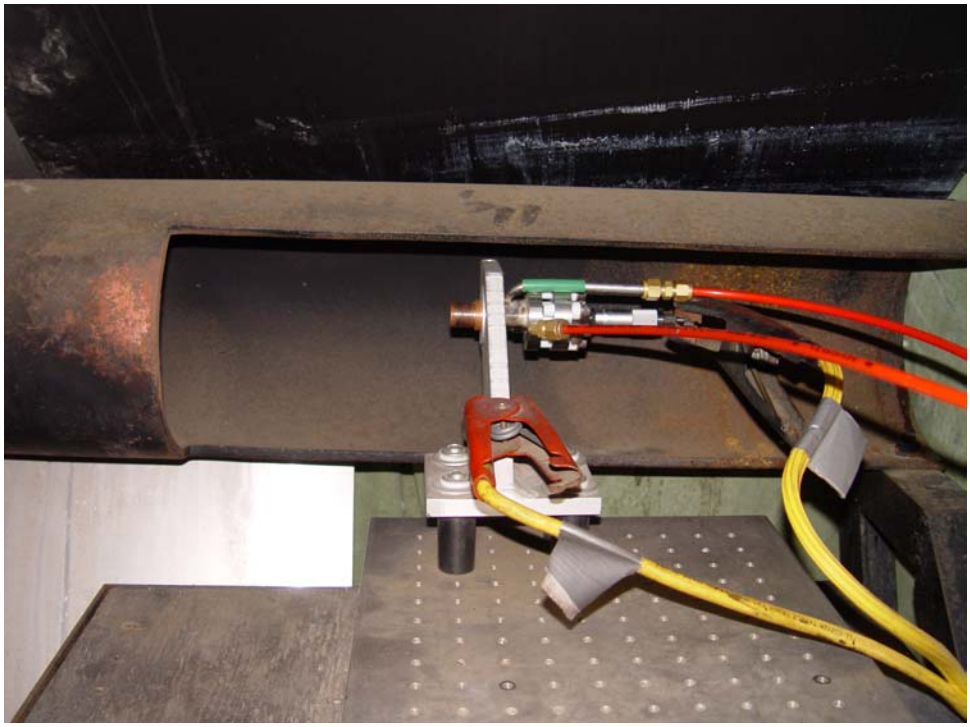

Figure 4.1: Photograph Showing the Plasma Porch in the Quiescent Test Cell

4.1.2. Virginia Tech Supersonic Wind Tunnel

The Virginia Tech blow-down, unheated supersonic wind tunnel was also used in this research to determine if the plasma torch would ignite in Mach 2.4 conditions. Mach 2.4 cross-flows were used because it was within the range of the combustor Mach number of practical scramjets and an existing wind tunnel nozzle block was available. However, the generated wind tunnel environment did not simulate true scramjet combustor conditions as the flow in the supersonic wind tunnel was unheated. The working section of this tunnel was a 23-cm x 23-cm with a 30 cm long test section where the plasma torch was

mounted through the floor of the tunnel in a vertical position. A total temperature probe was located downstream of the plasma torch at a sampling station to collect the total temperature profile of the plasma torch plume, see Figure 4.2 [Gallimore 2001]. A fused silica window on each side of the test section allowed optical access to the plasma torch plume. Each test in the tunnel lasted approximately 15 seconds. The freestream total pressure was approximately 381 kPa and a freestream total temperature was 285 K which corresponds to a freestream velocity of 554 m/s. A photograph of the Virginia Tech Supersonic Wind Tunnel can be seen in Figure 4.3.

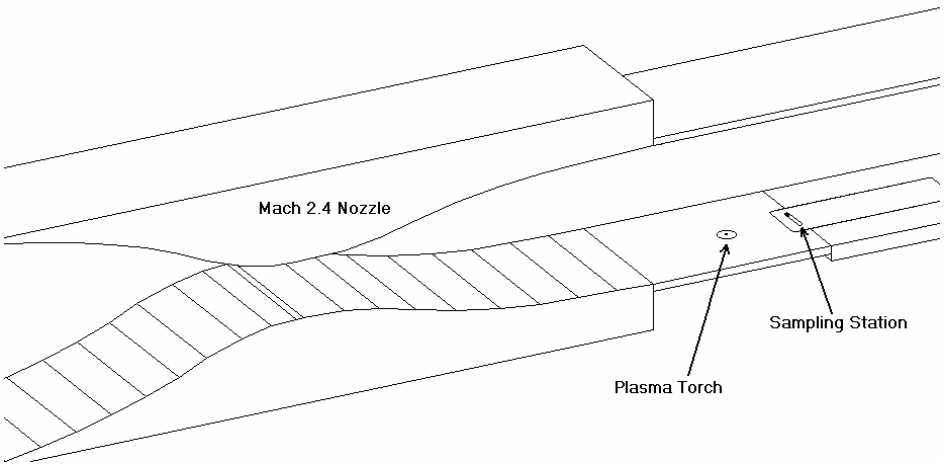

Figure 4.2: Schematic of the Virginia Tech Supersonic Wind Tunnel Experimental Set-Up [Gallimore 2001]

Figure 4.3: Photograph of the Virginia Tech Supersonic Wind Tunnel

4.1.3. The Power System

Three Miller Electric constant current, DC, SR-150-32 welders were wired in series to provide the power needed to run the plasma torch. The current supplied by the welders to the plasma torch was controlled by a dial on each welder that was adjusted before each run. The total open circuit voltage of the welder system was approximately 210 volts and the welders were capable of producing a current of 5 amps to 150 amps. An external high frequency starter (Miller Electric HF-251D-1) was activated by computer control for 0.25 seconds at the beginning of each run to start the plasma torch. The high frequency starter produced a short burst of high frequency current to initiate the electric arc. Once the torch was lit, the high frequency starter was turned off. Figure 4.4 shows photographs of the welders (A) and the high frequency starter (B) used.

(A) (B)

Figure 4.4: Miller Electric SR-150-32 Welders (A) and Miller Electric HF-251D-1 High Frequency Starter (B)

4.1.4. The Flow Measurement System

A Sierra Instruments 840M mass flow controller and a dual channel digital flow readout were used to control and monitor the flow rate of the feedstock gas. The flow controller was able to regulate the amount of gas passing through it based on the heating value of the gas. A built-in electromagnetic servo-controlled valve provided precise, instantaneous flow rate control. A photograph of the flow control system can be seen in Figure 4.5.

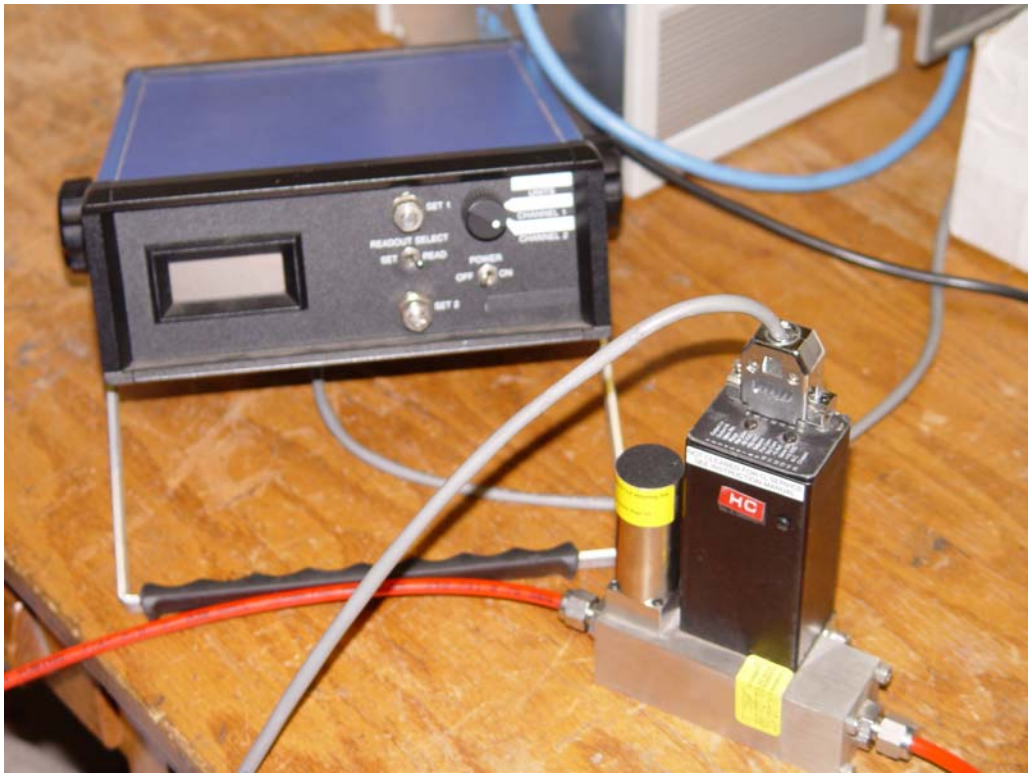

Figure 4.5: Sierra Instruments Flow Controller and Digital Readout

4.1.5. The Data Acquisition System

The data acquisition system is a collection of components and will be discussed in several sub-sections, including the spectrometer, the spectrometer traverse, total temperature probes, a high speed digital camera with filters and methods of collecting electrical measurements.

4.1.5.1. The Spectrometer

The CCD (charged-coupled device) spectrometer system utilized three Ocean Optics S2000 spectrometers. A 1.0 mm diameter viewing scope at the end of the combined fiber optic lines acted as a Gershun tube which reduced the viewing area of the spectrometer and reduced the amount of the reflected light entering the assembly. The scope was fitted with a 2 mm collimating lens, through which the photons were focused onto the fiber optic cable. The fiber optic cable was then split three ways by a trifurcated splitter where each leg went to one of the S2000s. Each leg of the fiber optic cable had a spectral

resolution of 0.08 nm and covered one third of the total spectral range, which was 196 nm to 730 nm. The integration time was set to 40-ms for the hydrocarbon surrogate. Figure 4.6 shows the spectrometer and the traverse used to control the location of the spectrometer scope.

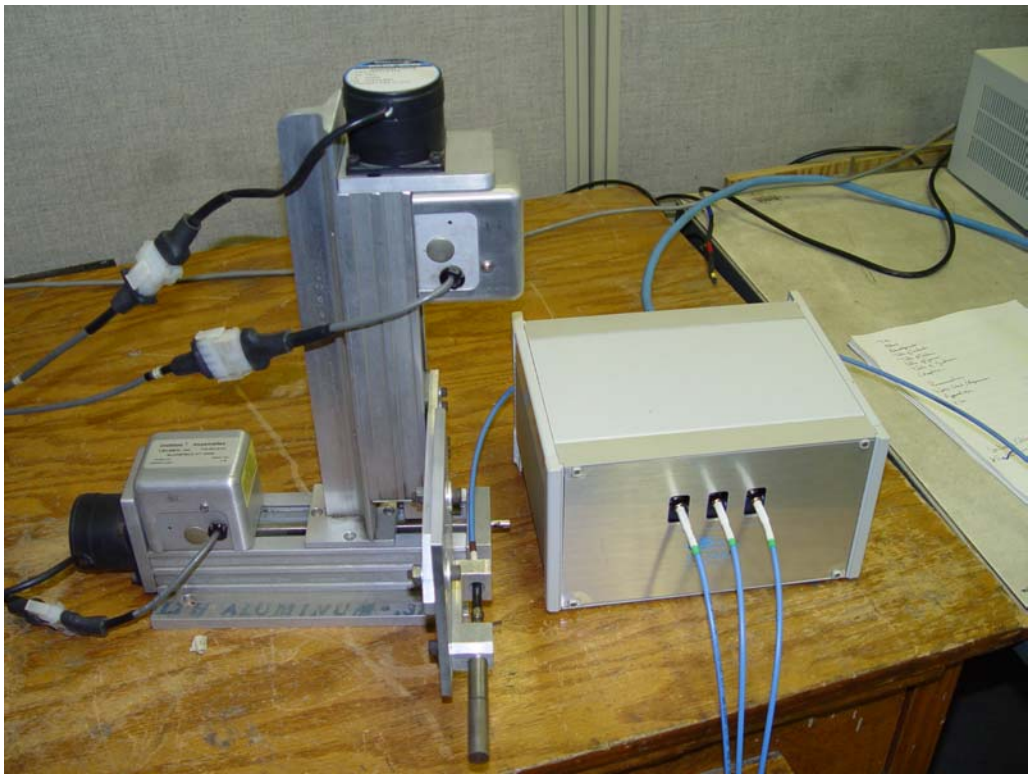

Figure 4.6: Ocean Optics S2000 Spectrometers and Velmex Unislide Traverse System Fitted with the Spectrometer Scope

The spectrometer system was calibrated using the recommended Ocean Optics HG-1 Mercury-Argon calibration light source. Figure 4.7 shows the calibration plot used to calibrate the spectrometer. The blue data is the data collected whereas the red Xs are the data given by Ocean Optics for the HG-1 light source. This calibration plot allowed for the calculation of the calibration coefficients required to run the Ocean Optics spectrometer control program in LabView. A note on the HG-1 calibration light source states that the wavelengths given (red X's) are intended as a quick, convenient reference and does not list every argon emission line that exists. This also explains why not every peak in Figure 4.7 is marked with a red X. Also, the peaks located at 508.08, 594.29, and

627.07 nm, are a result of a doubling effect of the 254.77, 296.73, and 313.16 nm wavelengths due to the lack of special filters in the spectrometer. The spectrometer data collected when the plasma torch was operated on the surrogate feedstock fuel fell within the range of 200 through 720 nm. Therefore any peaks that fell within the range of 200 through 360 nm could potentially be doubled due to aliasing and falsely appear between 400 and 720 nm. A detailed discussion of peaks that may exhibit the doubling effect can be found in Chapter 5.

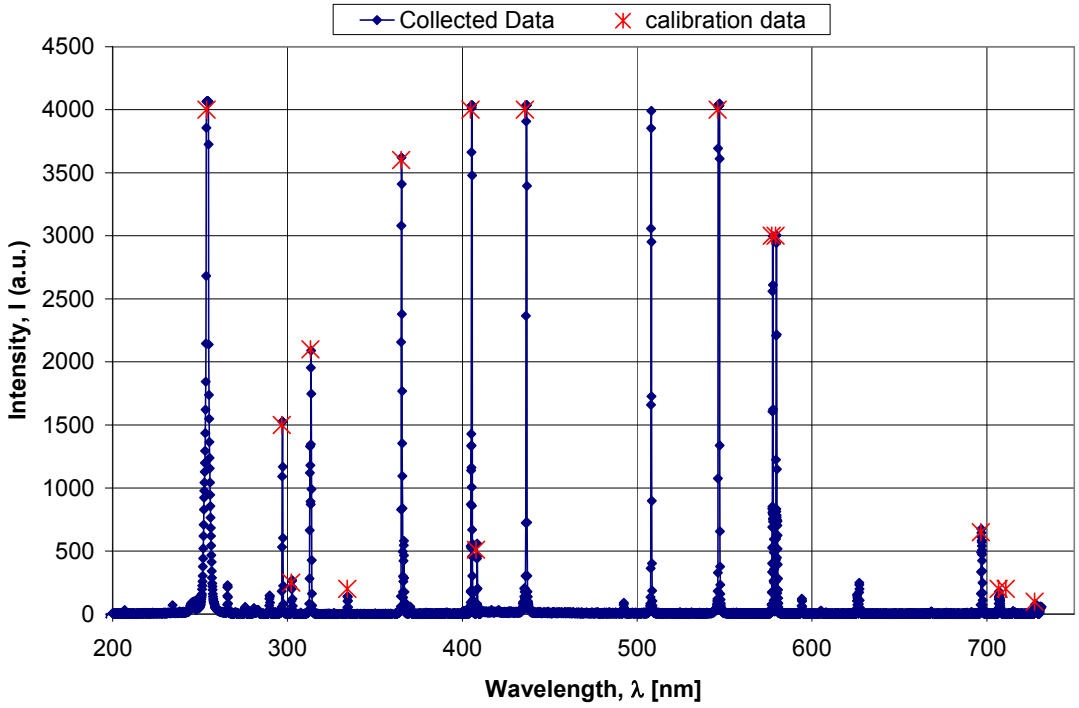

Figure 4.7: Mercury-Argon Calibration Plot used to Calibrate Spectrometer

4.1.5.2. The Spectrometer Traverse

The scope end of the spectrometer was attached to a traverse which was mounted to the optical table of the quiescent test cell. The traverse system consisted of a two-axis Velmex® MB2506KJ unislide which allowed for very fine adjustments in the x and y directions with accuracies of ± 10 μm. The traverse system was connected to a Velmex® dual-channel controller which was controlled by a LabVIEW program. See Figure 4.6 for a photograph of the Velmex Unislide traverse system.

4.1.5.3. The Total Temperature Probes

A probe located 7.6 cm downstream of the plasma torch plume was used to collect the temperature profile of the plume in Mach 2.4 conditions. The temperature probe consisted of three, exposed junction, 0.25 mm diameter, type-E thermocouples, arranged within a probe rake. The probe rake consisted of three 1.59 mm OD, 1.04 mm ID tubes spaced 6.4 mm apart. The recovery factor was calculated to be 0.95 [Gallimore 2001]. The rake was moved vertically from the floor of the tunnel to 3.8 cm above the floor of the tunnel by a motorized traverse for each run. The traverse was commanded to move the rake up one step and pause to allow the data acquisition program to collect a set number of data samples and then proceed to the next step until the rake reached the final predetermined height. Once the total temperatures were collected, they were then normalized with the freestream temperature and used to create the total temperature profiles. All thermocouples were calibrated by submerging the probe into a dish of ice water and a second reading was taken of the thermocouples in still air at room temperature near a glass bulb thermometer. The variations of the readings of the thermocouples were less than 3 %. Figure 4.8 shows an image of the triple total temperature probe (A) and the traverse system used to move the probe (B).

(A) (B)

Figure 4.8: Triple Total Temperature Probe (A) and Traverse (B)

4.1.5.4 The Pressure Transducers

Several pressure transducers were used to take pressure measurements throughout this work. The pressure transducers were used to collected pressure data of the upstream total pressure of the wind tunnel, the plenum pressure for the wind tunnel, and of the chamber pressure in the torch body. All pressure transducers used were calibrated with a dead weight tester prior to the test runs.

4.1.5.5. The Digital Camera and Filters

A Nikon D100 digital SLR camera was used to capture images of the plasma plume in the supersonic wind tunnel. The same lens was used for each exposure and the camera was mounted to a tripod and placed in the same location next to the tunnel for each test run. Therefore all of the images taken have the same scale. Some images were filtered to allow only certain wavelengths to pass through. Information regarding the band-pass filters used is shown in Table 4.1. Since the filters allowed a range of wavelengths to pass, there is a possibility that several species were present in the image. The corresponding specie listed in Table 4.1 is likely the most intense specie present in the given range as determined by the spectroscopic data taken with the spectrometer. Due to the ability of the filters to block out most visible wavelengths, the camera was focused on an object placed at the torch exit prior to the attachment of the filter to the camera. Great care was taken to prevent the settings from changing when the filter mount was installed after the focus had been set.

Table 4.1: Band Pass Filters Used in Digital Imagery

Brand	Center Wavelength (nm)	Half Bandwidth (nm)	Corresponding Specie	Shutter Speed
Ealing-Electro Optics	431.4	8.1	CH	1/500
Ealing-Electro Optics	515.1	8.8	C_2	1/800
Ealing-Electro Optics	656.7	11.1	H	1/500

4.1.5.6. Electrical Measurements

Current and voltage readings were taken for each run to determine the amount of power used to ignite the torch. Each signal was passed through an isolator board to reduce the magnitude of the signals before sending it on to the computer data acquisition program. All cables used to measure the current and voltage readings were kept as short as possible and isolated from other cables to reduce the amount of noise transmitted by the signals in the cables.

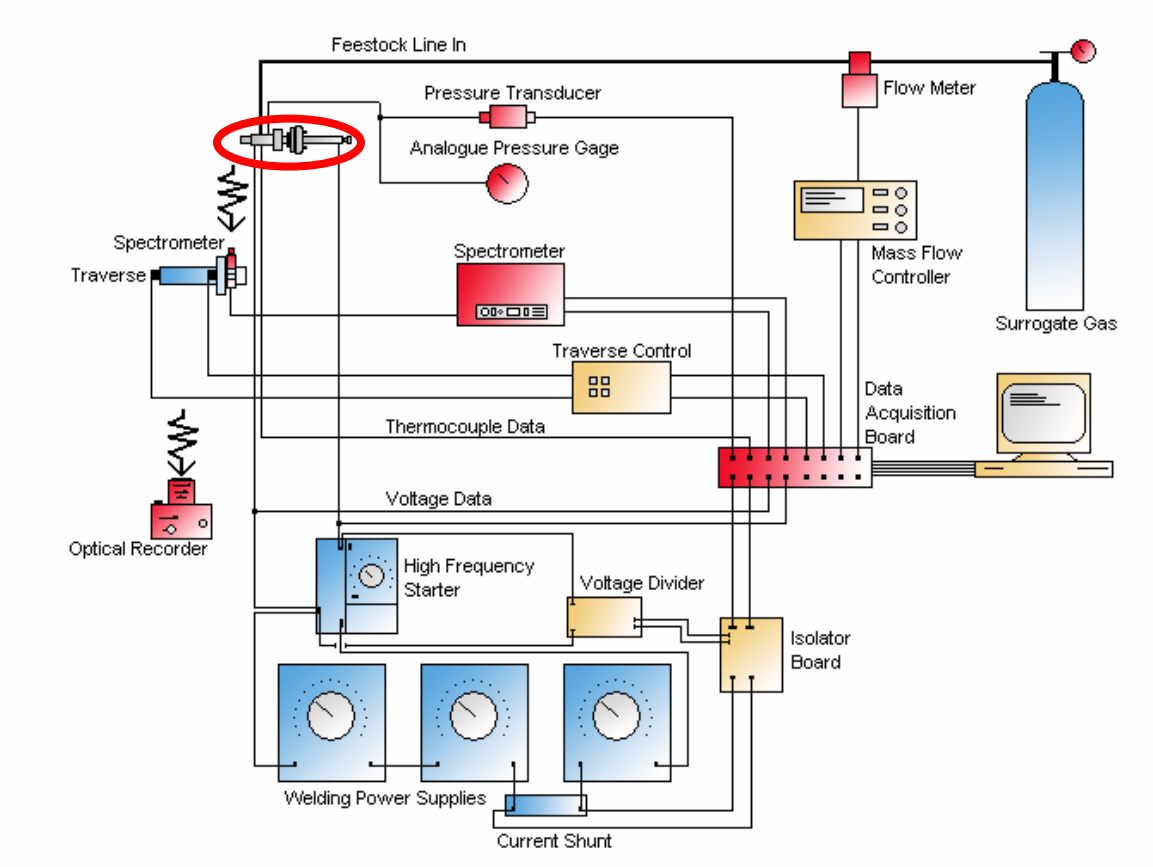

Figure 4.9: JP-7 Surrogate Plasma Torch Experimental Arrangement (Plasma torch circled in red)

4.2. Experimental Procedures

Tests were conducted in both quiescent and supersonic environments and similar procedures had to be followed for both test conditions. Spectrometer data were collected

in both environments to determine if the same species appeared in each. Once it was determined that similar species existed in each environment, a more detail analysis as to how variations in the parameters may have affected the spectrograms was conducted in the quiescent environment due to the ease of set-up and abundance of space available for the spectrometer system. This section discusses the procedures needed to prepare the torch and the spectrometer.

4.2.1. Torch Preparation

To prepare the torch for a test run, several steps were required before ignition could occur. The electrodes were checked for severe erosion since the torch would not ignite if too much of either electrode had worn away. Once the electrodes were deemed satisfactory for ignition, the gap between the electrodes was set. The micrometer drive was turned until the cathode made electrical contact with the anode. The cathode was then turn back until the electrical contact was broken. The cathode was then turned back an additional 0.178 mm to set the gap. Jumper-cable styled clamps were then carefully attached to each electrode taking care not to disturb the micrometer setting. After all connections were set, the feedstock gas valve was opened and the LabView program controlling the entire test run was started.

4.2.2. Spectrometer Data Acquisition

An Ocean Optics HG-1 Mercury-Argon light source was used to calibrate the spectrometer. This calibration was completed at the beginning of the quiescent test matrix and provided the calibration coefficients for the LabView spectrometer control program. Once the torch had been set up for a run in the quiescent environment, the spectrometer needed alignment and focusing. A hand-held light source was used to determine the focal area of the spectrometer as well as to determine if the collimating lens was focused for the distance being used. This alignment and focusing of the spectrometer had to be completed each time the spectrometer was moved off of the optical table. A distance of 15 cm between the plasma plume and the aperture of the

collimating lens was used in all quiescent spectrometer tests. For supersonic wind tunnel tests, the distance from the center of the wind tunnel, where the torch exit was located, to the aperture of the spectrometer was a distance of 17 cm. The larger distance used in the supersonic wind tunnel tests were due to the width of the tunnel, the thick glass doors, and the wind tunnel door hinges that obstructed some of the movement of the spectrometer traverse.

The LabView spectrometer control program not only controlled the spectrometer, but also the Velmex® MB2506KJ unislide traverse system to which the spectrometer was attached. Data were collected across the plume similar to that shown in Figure 4.10. In a single test run, several steps of the traverse allowed the spectrometer to collect data at several locations across the plume. For supersonic tests, configuration (A) was used due to the physical restrictions of the wind tunnel. The representation of the plume in this image is bent to show the effect of the cross flow, in this diagram, from top to bottom. In quiescent test cases, the schematic shown in Figure 4.10 (B) was used. The distance between each station (labeled 1 through 4) in Figure 4.10 (A) and (B) was 4.125 mm. The spectrometer aperture was set up at a normal angle to the plasma plume to allow a direct view of the plume in both test scenarios.

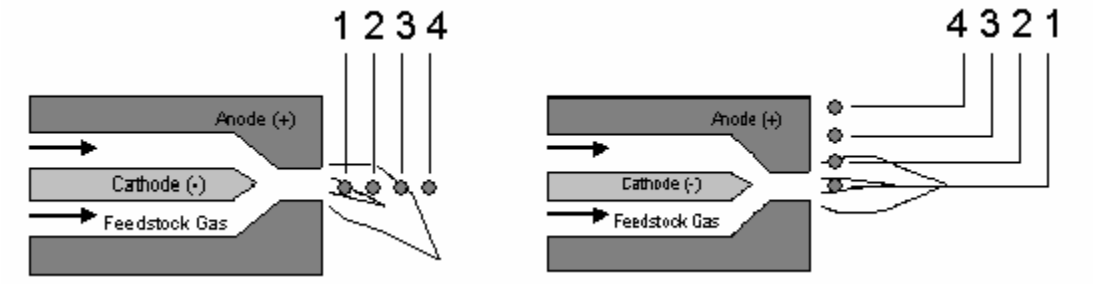

(A) (B)

Figure 4.10: Plasma Torch Centerline Profile Used in the Supersonic Environment (A) and Base Profile Used in the Quiescent Environment (B) for Spectrometer Measurements

4.3. Test Procedures

Each test set up was slightly different and therefore required slightly different test procedures. This section will briefly discuss the steps involved for each environment as well as a test matrix and the factors that determined a successful run. The data collected were analyzed in Excel and Tecplot.

4.3.1. Quiescent Environment

In the quiescent environment, the data acquisition program first sent a signal to the flow controller to allow the feedstock gas to pass through the torch. It then proceeded to turn the welders on and to temporarily (0.25 sec) turn on the high frequency starter to initiate the electric arc. As soon as the torch had started, torch chamber pressure, feedstock flow rate, voltage and current data were recorded. Two seconds were allowed to pass to allow the torch to stabilize before continuing to collect other data. LabView then sent signals to the spectrometer to take data between movements in the Velmex® traverse. After the traverse had moved its predetermined number of steps, it was returned to the home position, the welders turned off, the feedstock turned off and the program ended.

4.3.2. Supersonic Environment

The supersonic environment data acquisition program was similar to the quiescent program described in 4.3.1. Just as the quiescent program, the supersonic program began by turning on the gas to the torch. The welders were turned on and then the program proceeded to send a signal to the supersonic wind tunnel to open the valve which started the tunnel. Total pressure and temperature data of the tunnel was collected during the entire time the tunnel was running. After three seconds, to allow the tunnel to stabilize, the high frequency starter was turned on for 0.25 sec to start the torch. Torch chamber pressure, feedstock flow rate, voltage and current of the torch were collected while the torch was operating. The torch was given time to stabilize, as in the quiescent

environment, then the program began to collect the total temperature profile at the probe location 7.6 cm downstream of the torch. A traverse moved the total temperature probes in the vertical direction up to 3.8 cm in 29 steps. When applicable, spectroscopic data were also collected at this time. After all the data had been collected, the traverse returned to the home position, the welders and feedstock gas were turned off and the tunnel valve closed.

4.3.3. The Test Matrix

Half of the tests reported here were conducted in the quiescent environment and half were conducted in the supersonic wind tunnel at Mach 2.4 with a freestream total pressure of 381 kPa. While in the quiescent environment, spectrograms of the torch plume were collected. When the torch was run in the supersonic wind tunnel, total temperature profiles were collected 7.6 cm downstream of the torch exit and spectrograms of the plume were collected. For the total temperature ratio data, the torch was run in six combinations of flow rate and power as shown in Table 4.2.

Table 4.2: Test Matrix Used to Collect Total Temperature Data

Test	Flow Rate (slpm)	Power (W)
1	20	3000
2	20	3500
3	20	4000
4	25	3000
5	25	3500
6	25	4000

As with any experimental testing, there were many variables that can change from run to run. Therefore a method was needed to determine if a successful run had occurred. The first variable to be considered was the torch power. The torch power drifted between runs due to the erosion of the electrodes which varied the arc length. If the torch power was within 10% of the objective, then the next variable was analyzed. The next variable was the feedstock flowrate. The Sierra Instruments flow controller was very stable such that the flow rate did not change considerably from run to run. A feedstock flowrate

within 5% of the objective was considered to be a success. For the supersonic wind tunnel tests, the freestream tunnel pressure was also a variable that had to be considered. The freestream total pressure could vary up to 5% in a single run; therefore if the pressure was within 10% of the goal, the run was considered a success. There were cases where we did not have a true success in terms of the planned operating parameters. However, since all data is worth considering, there were some instances where the "unsuccessful" runs (i.e. the power was off target) will be presented as a comparison.

Chapter 5

Spectroscopic Studies

One way to determine the potential effectiveness of the plasma torch is to analyze a spectrogram of the plasma plume to determine what species are present. By doing so, one can determine if the feedstock is reacting with the freestream air as well as if there is truly combustion occurring due to the reactions of the plasma torch. In order to obtain data along the same plane, it was important to set up the spectrometer once and not move it until all data in a series was collected. This was possible in the quiescent test cell since the spectrometer and the plasma torch were mounted to the same optical table, therefore the majority of the spectrometer data presented was collected in that environment. Figure 5.1 shows unfiltered photographs of the plasma plume exhibiting typical plume shapes and sizes. Figure 5.1 (A) shows the plume in the quiescent environment whereas the Figure 5.1 (B) shows the plume in the supersonic environment with the flow going from left to right at Mach 2.4. The visible width in the image of the quiescent test cell is approximately 1.25 ft, but the spectral data collected was taken near the torch exit, the most luminescent area.

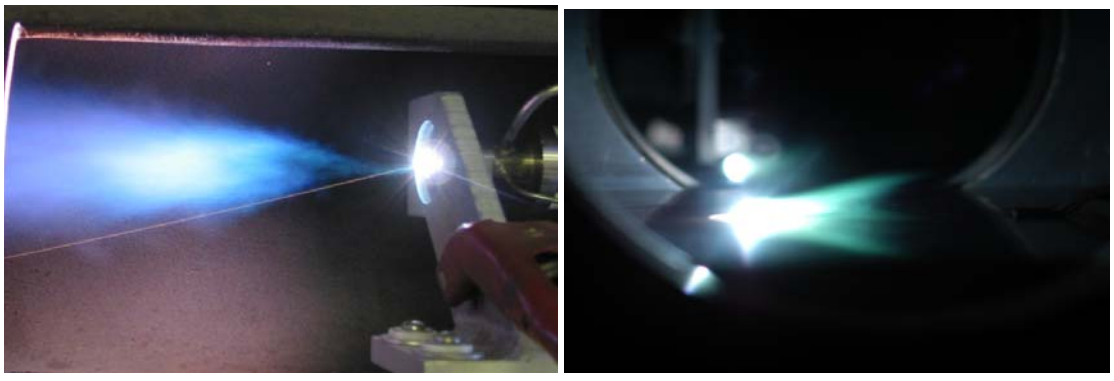

(A) (B)

Figure 5.1: Plasma Torch Operating on JP-7 Surrogate Feedstock
(A – Quiescent; B – Supersonic flow from left to right)

It is important to note that the integration time plays a key role in the relative intensities of each of the spectrograms. The integration time on the spectrometer, which is comparable to an exposure time on a camera, determines how long it will sample the plume; the higher the integration time, the longer it collects data. The lower the integration time, the less intense the sample will appear due to less light collected for that run. For the tests to determine if power played a role in species production, the integration time used was 20 ms. For the tests to determine how the species varied across the plume, an integration time of 40 ms was used. A more detailed discussion of each series of tests will follow.

Since integration times may differ between spectrograms, the intensities of similar spectral peaks will also vary between spectrograms. As long as the spectrometer was set up in a similar configuration for test cases to be evaluated against each other, the same spectral line in each comparable spectrogram can be relatively compared. However, two spectral peaks even within the same spectrogram can not be compared since the intensity levels of the spectrometer were not calibrated. Also, due to the lack of intensity calibration, the values given along the intensity axis do not correspond to the actual intensity values and only can be used for magnitude comparison.

Hydrocarbon-based plasmas have been found to contain a high concentration of hydrogen radicals, which are good combustion-enhancing radicals [Kimura et al. 1981]. Even though the hydrogen radical has been shown to be a beneficial combustion-enhancing specie, other less important species may play a key role in mechanisms that produce more combustion enhancing radicals, such as hydrogen, nitrogen, and oxygen.

5.1. A Detailed Analysis of the Spectrogram

Since the surrogate fuel consists of a mixture of hydrocarbons, it is expected that the spectrogram will be similar to other hydrocarbon spectrograms. A typical spectrogram

taken when operating with the surrogate fuel at the location closest to the torch exit is shown in Figure 5.2. This plume was produced when the torch was operated at 2.7 kW and with 30 SLPM of surrogate feedstock in the quiescent environment. Some species of interest are easily identified on this graph and are labeled accordingly. Identification of molecular and atomic species were made by comparing observed spectral data with compiled lists of known spectral lines [Pearse, 1976; Gaydon, 1974]. Identified hydrocarbon fragments include C, C_2, CH, H_2, and H. Also, the hydrocarbon-based surrogate fuel reacted with surrounding air to produced CN. The surrogate spectrogram shows little difference from the methane (Figure 5.3) and ethylene (Figure 5.4) spectrograms presented by Gallimore [2001] in regards to the species present.

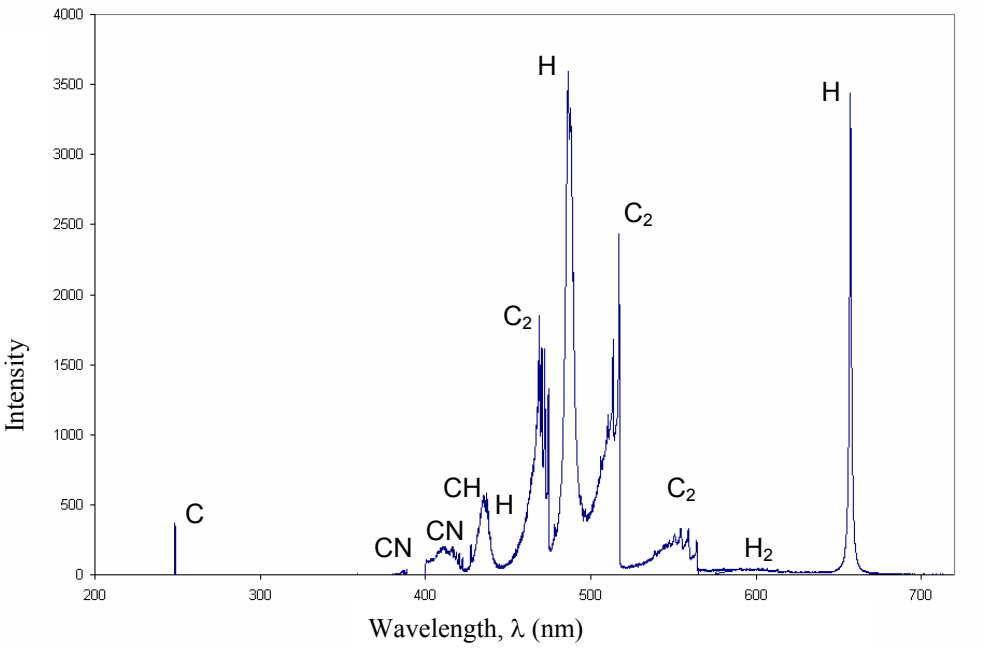

Figure 5.2: A Typical Spectrogram of the Surrogate Fuel; Taken at 30 SLPM, 2.7 kW, and with a Spectrometer Integration Time of 20 ms

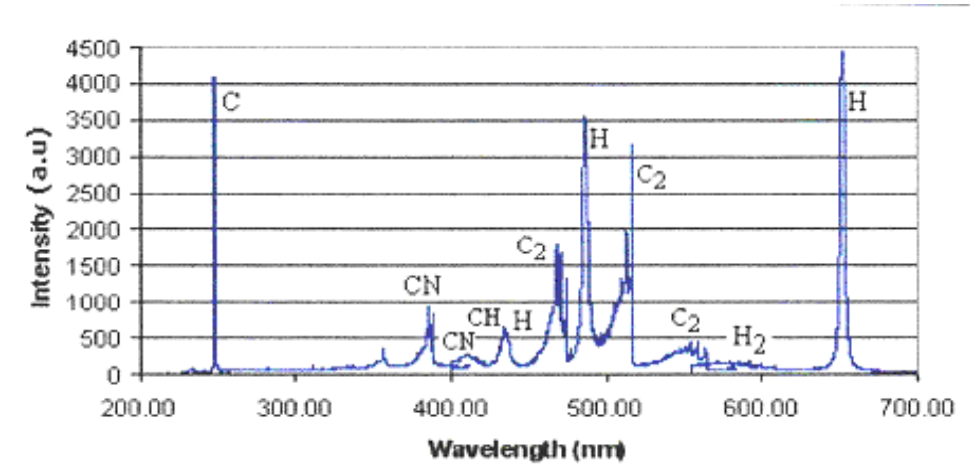

Figure 5.3: Methane Spectrogram; Taken at 0.5 g/s, 2.49 kW,
and with a Spectrometer Integration Time of 40ms [Gallimore 2001]

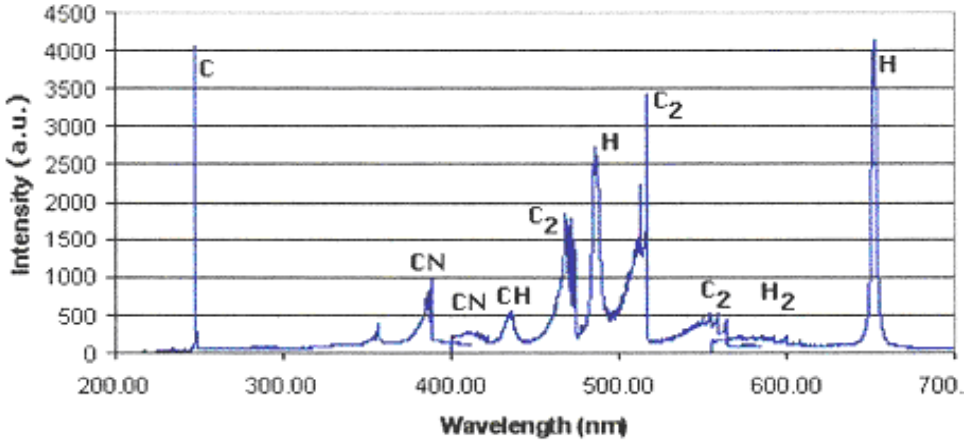

Figure 5.4: Ethylene Spectrogram; Taken at 0.5 g/s, 3.15 kW,
and with a Spectrometer Integration Time of 20 ms [Gallimore 2001]

One difference in the spectrograms shown in Figures 5.2 through 5.4 is that of the atomic carbon line C at 247.8 nm. Each of the single-hydrocarbon spectrograms (methane and ethylene) shows a very strong peak, but the surrogate had a lower peak when comparing the same carbon line among all the spectrograms. The difference in intensities of this spectral line could have been due to the surrogate fuel consisting of a mixture of methane, ethane, and ethylene and therefore having a different set of reaction mechanisms than the single hydrocarbon reaction mechanisms.

As stated in the previous chapter, there was a possibility that doubling may have occurred in the spectroscopic signal. Signals ranging from 200 through 360 nm needed to be considered when taking into account the possibility of doubling. After analyzing all of the spectroscopic data collected, the only peak that occurred in the questionable range was that of the carbon line located at 247.8 nm. If this peak doubled due to aliasing, the second peak would occur at 495.6 nm and would be significantly smaller due to the low intensity of the original peak at 247.8 nm. There were relatively large peaks close to 495.6 nm which would overshadow the aliased peak generated by the wavelength in question, therefore the doubling phenomenon, though it may have occurred, did not significantly alter the final spectrograms by creating false peaks.

Another strong specie that appeared in the spectrograms was that of carbon, in particular, the C_2 Swan bands near 473.7 and 516.52 nm and the C^+ peak at 427nm (Figures 5.5 and 5.8). Swan band systems occur frequently in sources containing carbon and are caused by the $A^3\Pi_g - X^3\Pi_u$ transition [Pearse, 1976; Gaydon, 1974]. In the surrogate fuel spectrogram, the C_2 spectral lines were relatively more intense than those in the methane and ethylene spectrograms. Also, the single hydrocarbon spectrograms did not appear to contain the 426.7 nm C^+ peak at all. When evaluating the spectral lines of C_2, C^+, and C in each of the spectrograms, it became clear that the mechanism responsible for creating atomic carbon in the surrogate plume appeared to be slower than when methane or ethylene were used. Upon closer inspection of the C_2 spectral lines, shown in Figure 5.5 (A), the common Swan band system near 473.7 and 516.5 nm stood out. The lines surrounding 516.5 nm clearly show the characteristic violet degradation of the Swan band system. Another example of violet degradation occurred near 558.5-nm shown in Figure 5.5 (B). A Swan peak characteristic of high pressure interactions occurred at 468.02 nm and was buried within other C_2 lines, making it difficult to notice upon first inspection.

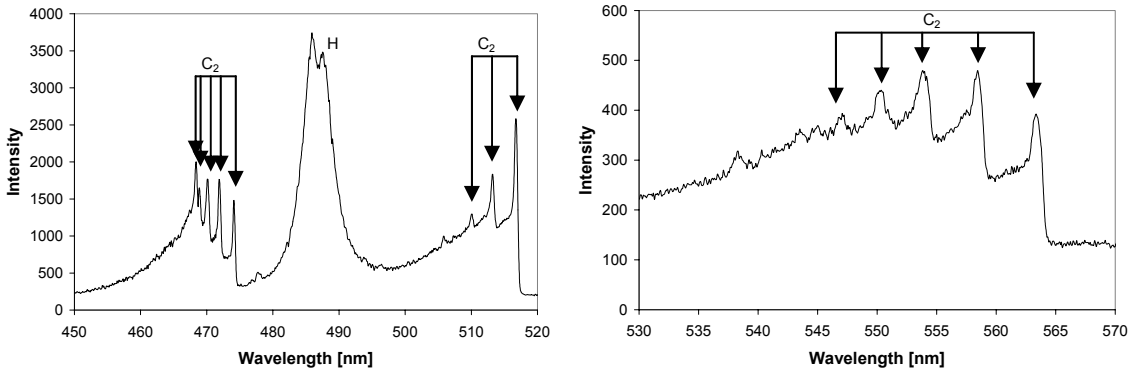

(A) (B)

Figure 5.5: C_2 Swan Band Systems; Taken at 30 SLPM, 2.7 kW, and with a Spectrometer Integration Time of 20 ms

A photograph of the torch operating in the supersonic wind tunnel, taken with a shutter speed of 1/800 sec and with a band-pass filter allowing only the wavelengths centered at 515.1 nm to pass through, is shown in Figure 5.6. This photograph, along with all supersonic photographs presented, can be compared to Figure 5.1 (B) for a frame of reference. Since the only peak in that region of wavelengths is one of the C_2 bands, this photograph is a representation of the presence of C_2. A sizable portion of the photograph shows a green haze around the bright center. This haziness comes from reflections off of the floor of the test section as well as pixel leakage due to the digital camera used to take the image. The important part of the photograph to consider is the bright spot in the center of the image and the plume shape. This is the part of the plume that contains the plasma arc as well as the wavelengths allowed to pass through the filter. Due to the fluid forces caused by the Mach 2.4 crossflows (from left to right in the figure), the plume appears elongated downstream of the torch exit. Also, since the plume appears to be parallel to the floor of the wind tunnel test section, this suggests that the penetration height of the plume is at a minimum. A better understanding of the penetration height can be determined from the downstream total temperature data presented in Section 6.2.

Figure 5.6: Filtered Photograph Representing C_2 with a Shutter Speed of 1/800 seconds and a Band Pass Filter Centered at 515.1 nm

Another well-defined set of peaks that appeared in all of the spectrograms are those of the monatomic hydrogen Balmer Series [Pearse, 1976; Gaydon, 1974]. Figures 5.2 through 5.4 show the H_α peak at 656.3 nm as well as the H_β peak at 486.2 nm very clearly. The weaker H_γ peak at 434.1 nm was not as clearly seen in those figures, but in Figure 5.8, it was easier to identify. These strong hydrogen lines were almost always present in hydrocarbon flames and were extremely dominant as can be seen in Figures 5.2 through 5.4.

Filtered photographs representing the presence of hydrogen at 656 nm peak are shown in Figure 5.7. Again, refer to Figure 5.1 (B) for a frame of reference. As with all of the filtered photographs, only the brightest area of the image should be considered due to reflections in the wind tunnel and due to the saturation of one pixel well leaking into the adjacent pixel wells of the digital image causing the haziness surrounding the aureole. The flow was passing from left to right in the images and could be inferred by the plume being slightly bent over and leaning to the right in all of the images. Since these images were taken manually, it could not be determined how much time had passed from one image to the next, but all three images were taken with a shutter speed of 1/500 sec and within the same run, meaning that none of the controllable variables have changed. It had been noted in previous work [Gallimore 2001] that the power supplied to the torch

contained oscillations found in the input voltage waveform at a frequency of 180 Hz. This oscillation is clearly present in the current work as can be seen from the images in Figure 5.7. Further research regarding this oscillatory behavior is being planned for future work.

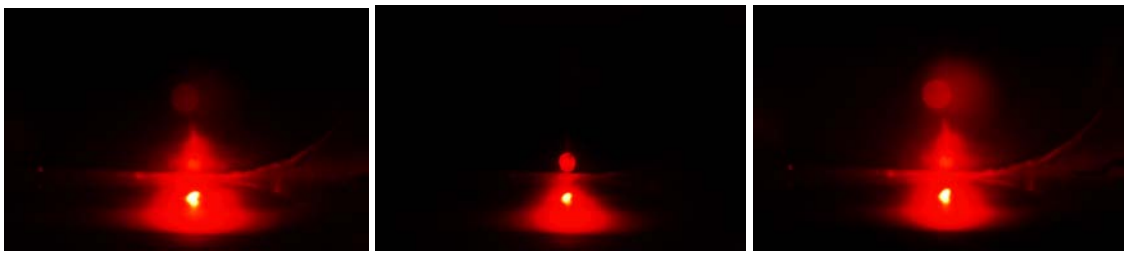

Figure 5.7: Filtered Photographs Representing H with a Shutter Speed of 1/500 seconds and a Band Pass Filter Centered at 656.7 nm

Another specie found in hydrocarbon plume was CH, which was readily excited during the combustion of hydrocarbons and in electrical discharges where carbon and hydrogen were involved. The Douglas-Herzberg system of CH [Pearse, 1976; Gaydon, 1974], with its characteristic undeveloped heads, was detected near 438 nm, as can be seen in Figure 5.8, and exhibits the expected red degradation. A filtered photograph, taken with a shutter speed of 1/500 sec, displayed wavelengths near 431-nm can be seen in Figure 5.9 and must be observed in a similar way as the other filtered photographs. This system can be attributed to the $A^1\Pi - X^1\Sigma$ transition.

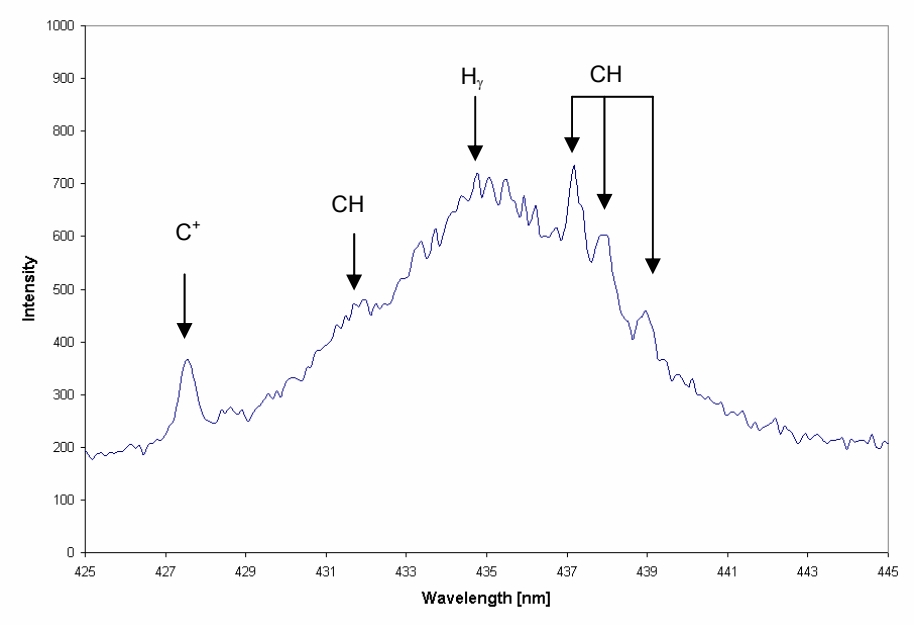

Figure 5.8: CH Spectral Lines and a Balmer Series H Line; Taken at 30 SLPM, 2.7 kW, and with a Spectrometer Integration Time of 20 ms

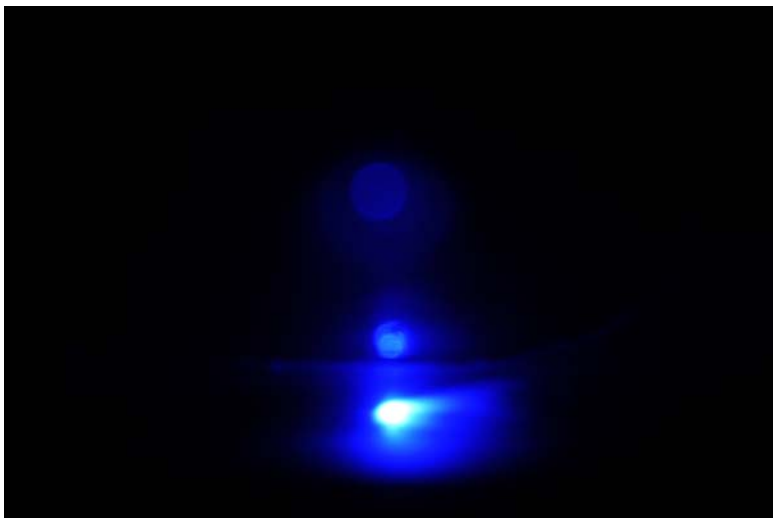

Figure 5.9: Filtered Photograph Representation of CH Specie with a Shutter Speed of 1/500 seconds and a Band Pass Filter Centered at 431.4 nm

As with any complex mixture of various species, there was band superposition. Band superposition is the phenomenon in which one system combines with another, making some peaks appear more intense than they really are. This is a frequently occurring phenomenon in samples containing closely radiating species. Figure 5.10 shows how spectral lines of CN and H_2 overlap making it very tedious to identify the peaks. CN

appeared when excited hydrocarbon species interacted with the surrounding atmosphere. The system shown in Figure 5.10 was of the CN Violet System, indicative of the $B^2\Sigma - X^2\Sigma$ transition. The CN system near 420 nm appeared to display red degradation, but that could be attributed to band superposition with the nearby Deslandres-D'Azumbuja C_2 system [Pearse, 1976; Gaydon, 1974].

H_2 appeared throughout the entire visible spectrum, but did so weakly, making it difficult to identify when other species were present. Diatomic hydrogen was identified near 420 nm (Figure 5.10) and weakly at 610 nm. When looking for the presence of hydrogen in a spectrogram, it is more common to look for the easily identified Balmer hydrogen lines as opposed to H_2 peaks, since H_2 does not resemble a usual band structure [Pearse 1976].

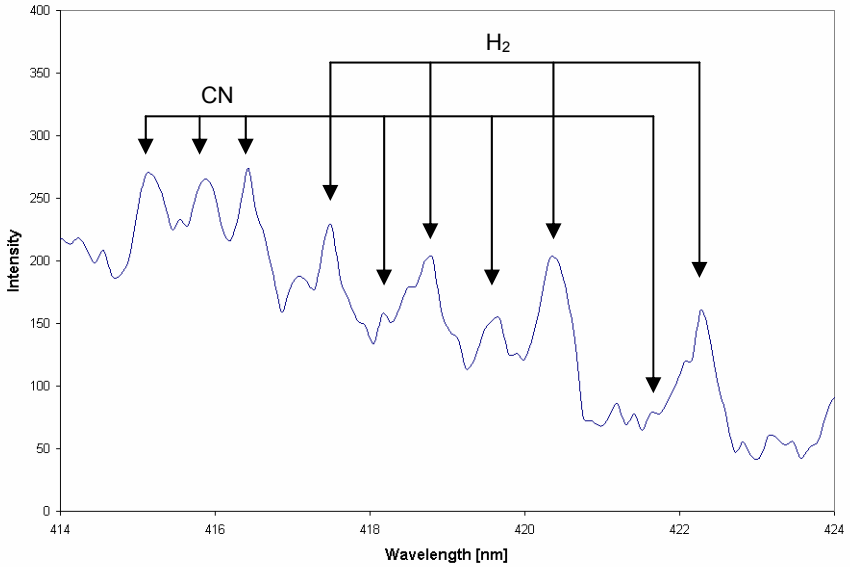

Figure 5.10: CN and H_2 Spectral Lines; Taken at 30 SLPM, 2.7 kW, and with a Spectrometer Integration Time of 20 ms

5.2. Study of How Power Affects the Spectrogram

An increase in the torch power has been found to exponentially increase the intensities of the downstream products for methane and nitrogen feedstocks [Gallimore 2003]. With

this information, a study was conducted to determine if the same holds true for the surrogate feedstock. The torch was run in the quiescent test cell at 2.7, 3.7, and 5.0 kW and a surrogate feedstock flow rate of 20 SLPM. The spectrometer integration time was set for 20 ms for all tests in order to be able to compare intensities. Figure 5.11 shows the three spectrograms at the varying power levels.

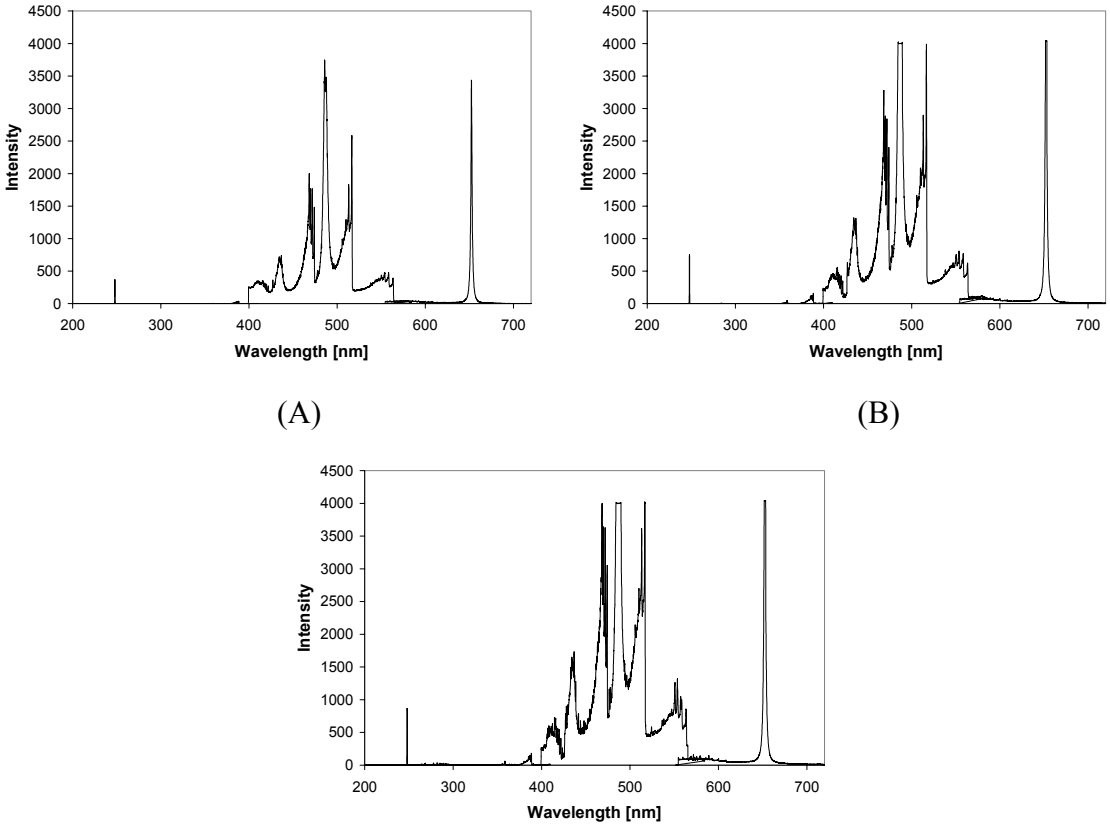

Figure 5.11: Spectrogram Comparisons of Varying Power; Taken with a Spectrometer Integration Time of 20 ms, 30 SLPM, and 2.7 kW (A); 3.7 kW (B); 5.0 kW (C)

Some clipping occurred on the two strongest hydrogen peaks at 3.7 kW and 5.0 kW, but analyzing any other specie will show that power did indeed affect the intensities of the species. Figure 5.12 shows how the intensity values increased as the power increased for a random set of peaks from the spectrograms shown in Figure 5.11. Not all of the peaks followed the same rate of change in intensities as the power increased. The trend for the peak at 554 nm appears to be almost linear whereas the rest of the data presented does not

appear as linear. This could signify that the power has a different affect on the rate at which the individual reaction mechanisms occur. The result to be drawn from this data is that, overall, the relative intensity value of each peak increases as the power increases.

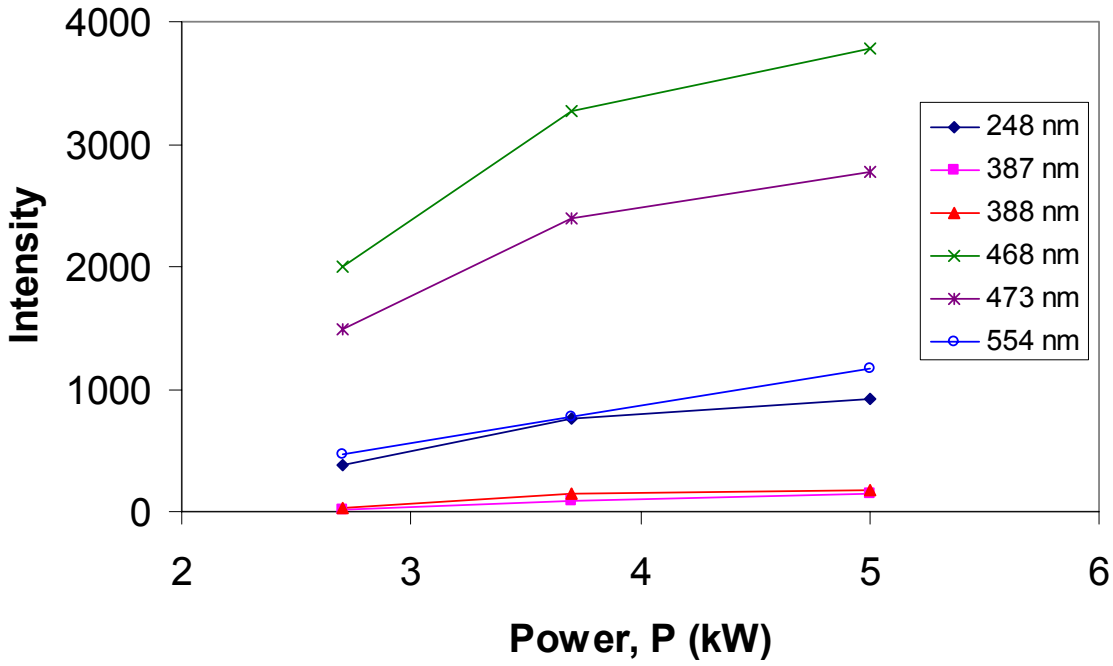

Figure 5.12: Relationship Between Power and Relative Spectrogram Intensities Taken from Quiescent Data Shown in Figure 5.11

5.3. Study of Species within the Plume

The location at the torch exit was the most luminescent location to collect spectroscopic data. This location in addition to the region of cooler gases surrounding the hot core is called the aureole. The core of the aureole is a region of intense chemical activity where there is such a high temperature that all gases are largely dissociated [Cobine 1958]. Due to this occurrence, the further from the core of the aureole data were collected, the lower the relative intensities became as can be seen in the discussion to follow. The species at various locations in the plume have been considered in both quiescent and supersonic

environments. In the quiescent environment, data were collected across the plane at the base of the torch shown in Figure 4.10 (B).

Upon detailed inspection of the species from the center of the plume (Figure 5.13 (A)), all of the species described in Section 5.1 are accounted for as expected. The spectrometer was set up to traverse across the entire base profile within a single run to maintain consistent operating conditions. A second spectrogram from the same run is shown in Figure 5.13 (B) using the same scale for comparison. The spectrogram in Figure 5.13 (B) was taken at 4.125 mm from the centerline of the plume. As one can see, the specie intensities decreased as the distance from the centerline increased. Also the relative intensities changed as the sample station moved from the centerline of the plume. The spectrogram in Figure 5.13 (A) shows peaks at varying intensities, whereas Figure 5.13 (B) shows peaks at about equal intensities, suggesting a lower concentration of species further from the torch exit. A lower concentration of species influences the rate of reaction; the lower the concentration, the slower the rate of reaction. Also, the locations of the peaks across the wavelength axis in both images in Figure 5.13 remain the same signifying that the species are not changing; only the intensity values are changing.

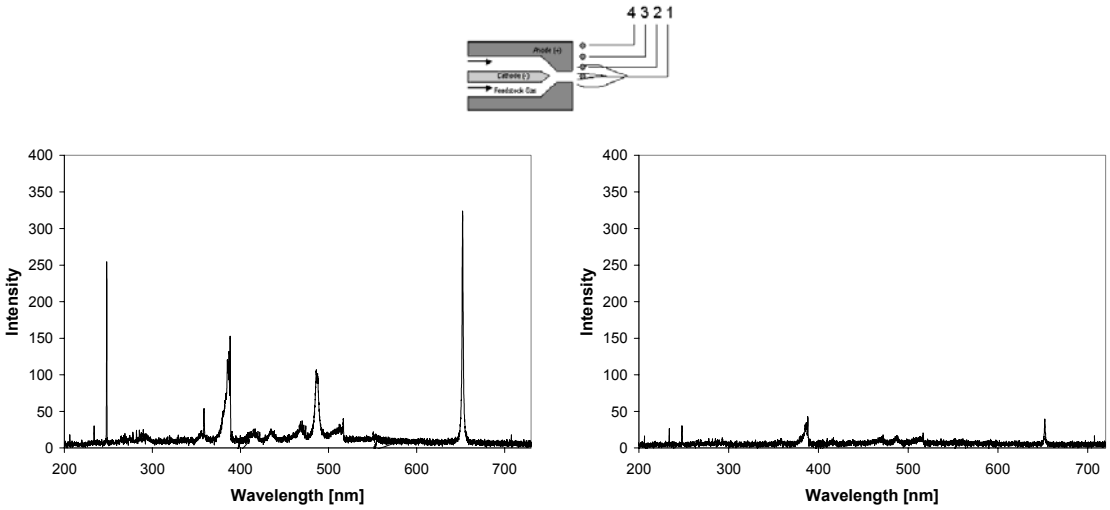

(A) (B)

Figure 5.13: Comparison of Spectrograms in Quiescent Environment; Taken at 30 SLPM, 2.7 kW, and with a Spectrometer Integration Time of 20 ms; (A) Station 1 and (B) Station 2

Another study was conducted to see how the species might change as the sample station moved across the plume in the supersonic environment. Data were collected across the plume similar to that shown in Figure 4.10 (A). Figure 5.14 shows two spectrograms; (A) is at the torch exit (the core of the aureole) and (B) is 8.25 mm up from the torch exit. Similar results occur here as they did in the quiescent study. The specie intensities decrease as the measurement station was moved further from the torch exit. Since the supersonic spectroscopic data were collected at a distance 2 mm greater than the quiescent spectroscopic data, it would be expected to see a greater decline in intensities than the quiescent sample exhibited. Due to the effect of the wind tunnel, the plume did not simply go straight out of the torch, rather, the supersonic cross flow forced it to bend downstream, making the area directly above the torch exit an interesting zone where the fuel interacted with the surrounding air. The dominant CN species in Figure 5.14 confirmed this. A complete set of the axial plume spectrometer data for both quiescent and supersonic flow is given in Appendix B.

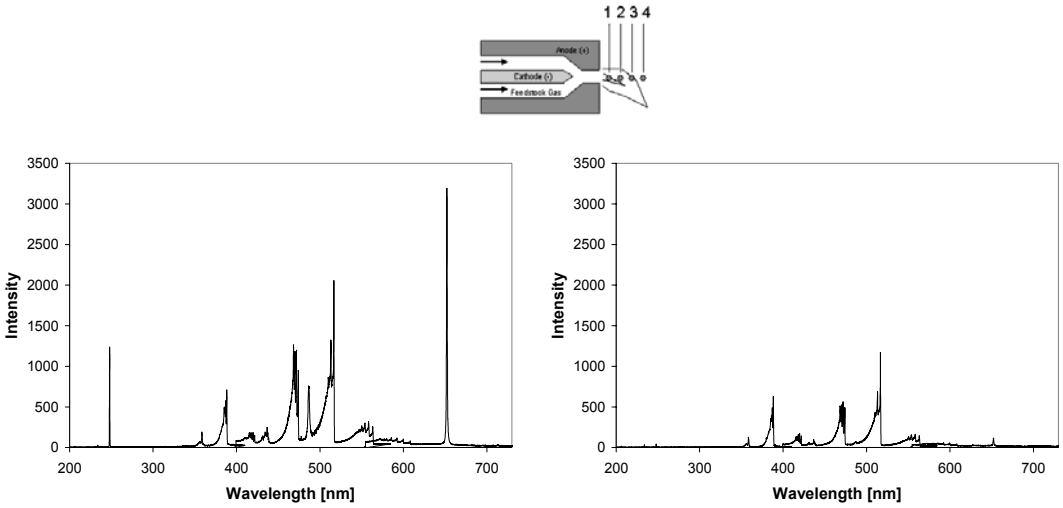

(A) (B)

Figure 5.14: Spectrogram of Surrogate in Supersonic Environment at (A) Station 1 and (B) Station 3; Taken at 30 SLPM, 2.7 kW, and with a Spectrometer Integration Time of 20 ms

5.4. Comparison of Supersonic to Quiescent Spectrograms

The purpose of the comparison made in this section was to determine if there were different species generated between the quiescent and the supersonic conditions. The quiescent test cell held the plasma torch in a horizontal orientation whereas the supersonic wind tunnel held the plasma torch in a vertical orientation. It had been said that if an arc burned in a horizontal position (quiescent orientation), then there would be buoyant forces due to the hot gases that can cause the arc column to arch and thus alter the length of the column even though the electrode gap remains unchanged. Electrode material will be lost at a fairly constant rate, but will often come off in drops which for short periods change the effective length of the column as well [Cobine 1958]. If possible, a new quiescent rig should be considered for future testing in order to make a more accurate comparison between the two test conditions.

The majority of the spectroscopic data presented here was conducted in the quiescent environment. Some spectroscopic data were collected in the supersonic environment for the purpose of comparison. Figure 5.15 shows spectrograms of the surrogate fuel in both the supersonic environment (A) and the quiescent environment (B). Both spectrograms were taken when the torch was operated with 4.0 kW of power and 20 SLPM of surrogate feedstock. Each of the spectrograms shown has the same scale for easier comparison. All of the species present in the quiescent environment were present in the supersonic environment. The only noticeable difference was CN near 358.5 nm denoted by the arrow in Figure 5.15 (A). This specie appeared in the quiescent spectrogram, but was not as strong as that seen in the supersonic spectrogram. The difference is thought to be due to a change in environments which caused the reaction mechanisms to alter slightly. With the addition of more air passing over the torch (Mach 2.4), there was a greater chance that the fuel will interact with the surrounding air. In the quiescent environment, the surrounding air was stationary. Therefore, once the air was consumed in the fuel-air interactions, replacement air was not immediately available to interact. In the supersonic environment, replacement air was constantly arriving due to the Mach 2.4 crossflow which allowed “new” air to always interact with the fuel coming out of the torch.

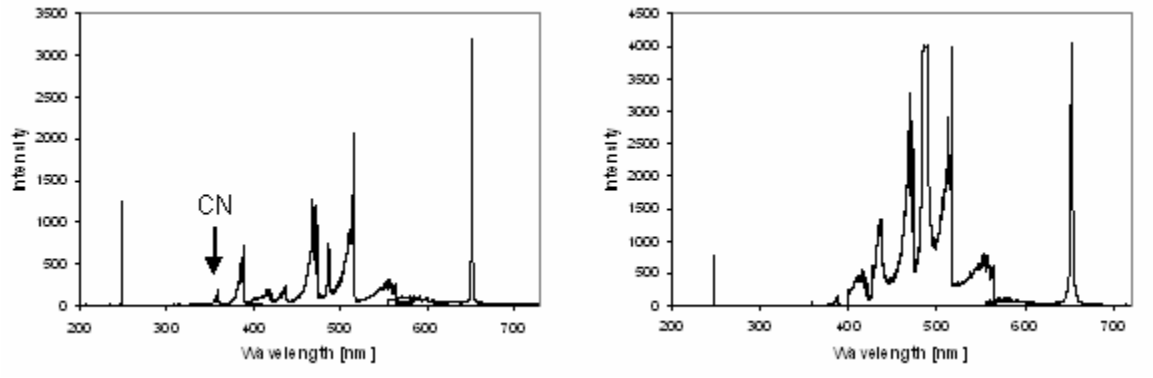

(A) (B)

Figure 5.15: Comparison of (A) Supersonic Spectrogram Taken at 20 SLPM, 4.0 kW, and with a Spectrometer Integration Time of 25 ms and (B) Quiescent Spectrogram Taken at 20 SLPM, 4.0 kW, and Spectrometer Integration Time of 20 ms

Most of the spectrogram peaks in the supersonic environment were relatively much lower than those in the quiescent environment. This was due to the shorter residence time that the fuel has in order to react. In the quiescent environment, the fuel had plenty of time to complete its reaction mechanisms and produce stronger peaks, whereas in the supersonic environment, there was an air flow interfering with the combustion region and preventing the fuel from igniting to its fullest potential. The slightly larger distance from the torch exit to the spectrometer scope in the supersonic environment could also decrease the relative peak intensities. From the results discussed in this section, it can be concluded that the data collected in the quiescent environment is sufficient in order to determine the identity of each species and to compare relative intensities as power, fuel flow rate, and location within the plume varies.

5.5. Electrode Erosion

Although there was not a spectrogram that showed signs of molybdenum, there was anode erosion occurring which was verified by inspection of the anode after each run. During the experiments, wide variations in the life of the torch anode were observed. Anode life was defined as the number of cold starts that could be completed with the anode. Anode failure was defined as an inability to establish the torch arc, even with the high frequency starter. In some test sequences, 30 cold starts were obtained. In others, as few as six starts were possible. The alignment of the cathode with respect to the anode has been known to be critical with respect to anode life. Care was taken to align the assembly as well as possible, but recent discussions and the above observations suggest that the alignment was not adequate.

It has been shown that when the current in the work flows symmetrically toward the arc, the arc is stable; see Figure 5.16 [Cobine 1958]. However, since the work is connected to the plasma torch via the feedstock supply line, the current acts as if it flowed toward the arc from one side. This creates a strong magnetic force which tends to push the arc attachment point to the location furthest from the feedstock supply line. In the supersonic environment, fluid forces were also applied to the arc causing the arc to attach at a downstream location on the anode. The magnetic force due the lack of symmetry of current flow may be overshadowed by the fluid forces caused by the cross flows of the wind tunnel, but for a robust plasma torch, the symmetry of the current should be evaluated prior to the redesign of the next generation plasma torch.

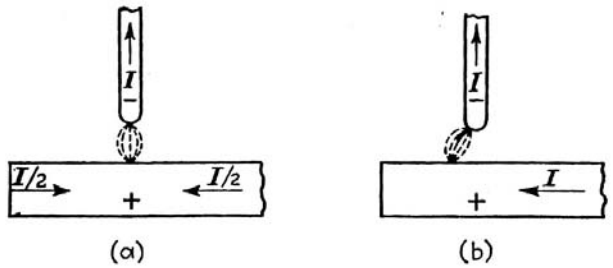

Figure 5.16: Effect of Arc-Current Magnetic Field on the Arc: (A) Symmetrical Flow to Arc and (B) Nonsymmetrical Flow to Arc [Cobine 1958]

In addition to alignment issues, the power setting plays a vital role in the longevity of the torch. Tests conducted during this work ranged from 3.0 to 4.0 kW with an occasional unplanned test that had a power setting as high as 5.0 kW. After each run completed, visual inspection of the torch electrodes were conducted to determine if the torch was in a satisfactory condition for a second run. It was noted that for higher power settings, the torch electrodes eroded more quickly than when the torch was operated at lower power settings. Recent discussions suggest that if the torch electrodes were meticulously aligned, the life of the electrodes would increase significantly across all power settings.

A filtered photograph of the plasma torch operating in the supersonic wind tunnel, shown in Figure 5.17, displays a clear image of the extremely luminescent eroded molybdenum particles downstream of the torch exit in the supersonic environment. During the run that this image was captured, there was a large amount of molybdenum anode loss which allowed identification of the trail as such. The filter used in this image allowed wavelengths close to 515 nm to pass through, but since the eroded particles were extremely bright and emitted white light, the light waves in the range of the filter were able to pass through and therefore appear in the image. All of the spectrograms were taken at the torch exit and did not contain any trace of eroded molybdenum since all of the eroded molybdenum was blown downstream and away from the sampled area.

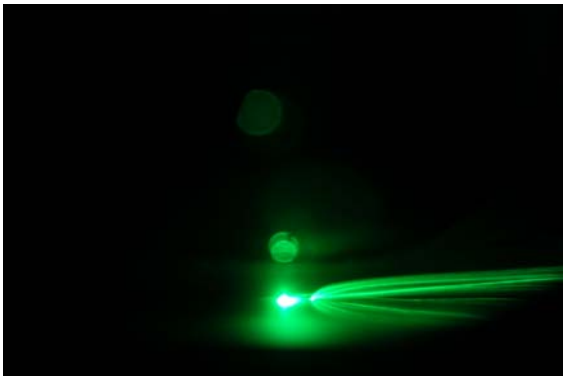

Figure 5.17: A Filtered Photograph Displaying Electrode Erosion in the Supersonic Environment with a Shutter Speed of 1/500 and a Band Pass Filter Centered at 515.1 nm

Chapter 6

Temperature Profiles

To determine how the plasma torch operated in the supersonic environment, a qualitative data analysis was conducted. The data of interest was that of the total temperature located downstream of the torch which was operated at various flow rates and power settings in the Mach 2.4 supersonic wind tunnel. Each test in the tunnel lasted approximately 15 seconds. The total freestream pressure was approximately 381 kPa and a freestream total temperature was 285 K, which corresponded to a freestream velocity of 554 m/s.

A triple thermocouple probe (Section 4.1.5.3) located 7.6 cm downstream of the torch exit collected three total temperature profiles spaced 6.4 mm apart in a single run. In the run, the entire probe was traversed vertically to a height of 3.8 cm above the floor of the wind tunnel in 29 equal steps. In post processing, a total temperature ratio profile was constructed for each test case and will be presented in the following sections. The total temperature ratio is the total temperature at the sampling location downstream of the torch divided by the total temperature of the upstream freestream air during the same run.

6.1. The Temperature Profiles

Total temperature ratio profiles have been constructed for comparison between the various test conditions. For ease of comparison, all of the plots have been assembled with the same total temperature scale. Figure 6.1 shows the total temperature ratio of the torch operating at 20 SLPM and at powers of 3.0 (A), 3.5 (B), and 4.0 (C) kW. Figure 6.2 shows the total temperature ratio profile of the torch at 25 SLPM and at the same powers as mentioned above. The temperature profile data were collected in a single run

with the triple total temperature probe. Each probe was spaced 6.4 mm apart making the total width of the triple probe 12.8 mm. Both the x-axis and y-axis shown in Figures 6.1 and 6.2 have been normalized by the effective diameter of the torch exit.

By collecting the data in a single run, the small variations in freestream pressure, torch power, and oscillations within the plume were minimized. Even though the total temperature data did not cover a large horizontal area (Y/d_{eff}), what is presented represents the trends of the total temperature profile.

Upon examination of the total temperature ratio profiles in Figures 6.1 and 6.2, it can be seen that the maximum total temperature ratio increased as the power increased for each flow case. As the torch power was increased, more energy was available to assist with the reaction mechanisms and to raise the temperature of the plume. Many of the discussions to follow concentrate on the maximum total temperature ratio available from the data shown in Figures 6.1 and 6.2. Ideally, the total temperature profiles should show the boundaries of the maximum total temperature ratio for each test condition. Therefore, what is shown is a representation of the trends to be expected for each test condition.

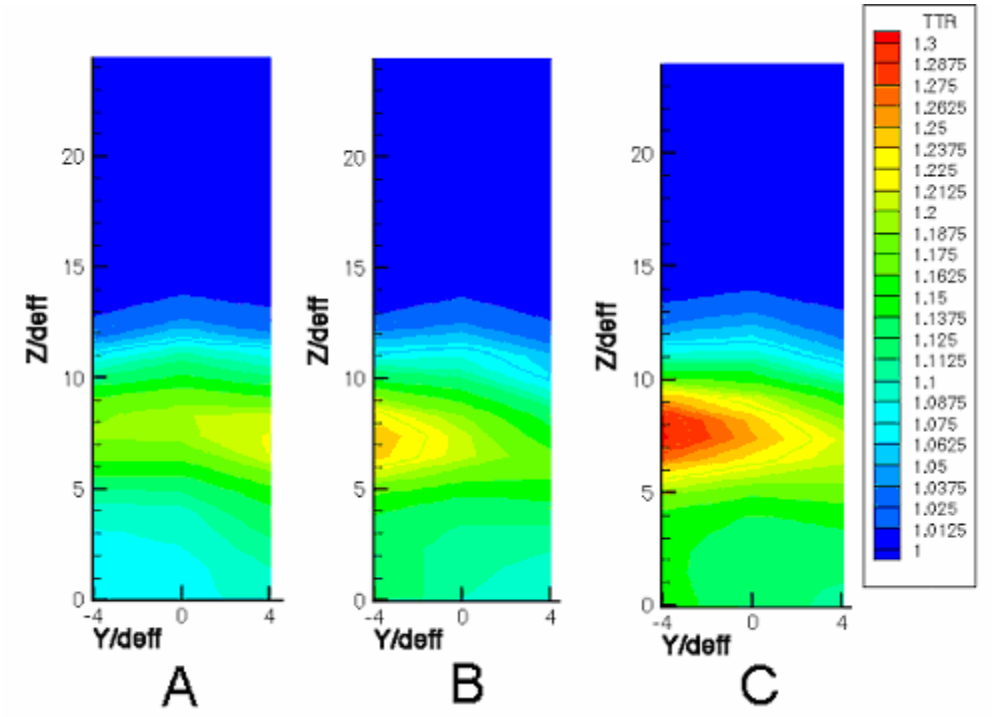

Figure 6.1: Total Temperature Profiles for Torch Operating at 20 SLPM at Increasing Powers of 3.0 (A), 3.5 (B), and 4.0 kW (C)

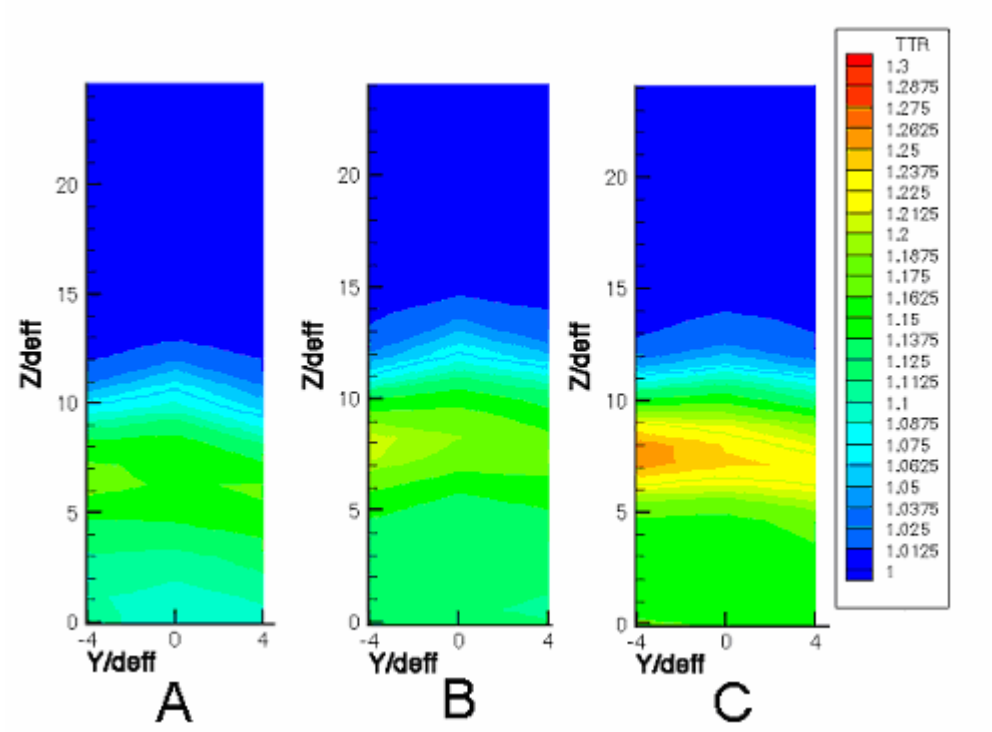

Figure 6.2: Total Temperature Profiles for Torch Operating at 25 SLPM at Increasing Powers of 3.0 (A), 3.5 (B), and 4.0 (C) kW

6.2. Penetration Height

For all six settings presented in Figures 6.1 and 6.2, the penetration height of the plume was represented by Z/d_{eff} and was approximately 7.0, where Z/d_{eff} was the height normalized by the effective diameter of the torch exit. The penetration height is defined as the normalized vertical height of the highest measured temperature within each temperature profile. Similarly, Y/d_{eff} was the horizontal distance normalized by the effective diameter of the torch exit. As a comparison, Gallimore [2001] had tested the plasma torch in a Mach 2.4 cross flow using ethylene at a momentum flux ratio of 1.14 and a power setting of 1.5 kW and found the total temperature profile to be that shown in Figure 6.3. This is the only torch alone ethylene temperature profile presented in the reference. Since the same torch design was used, the values of Z/d_{eff} and Y/d_{eff} were the same for all total temperature profiles presented here. The diameter of the anode constrictor remained constant in all cases.

Figure 6.1 included momentum flux ratios of 0.450 (A), 0.452 (B), and 0.471 (C) whereas Figure 6.2 included momentum flux ratios of 0.579 (A), 0.556 (B), and 0.503 (C). Even though the absolute maximum total temperature ratios were not clearly shown in Figures 6.1 and 6.2, the penetration heights appeared to be constant for each test case. Since the momentum flux ratios of Figures 6.1 and 6.2 were much lower than that of Figure 6.3, it would be expected that the penetration heights would be respectively lower than those shown in Figure 6.3. Also, the power setting used for the data of Figure 6.3 was much lower than the powers used in Figures 6.1 and 6.2. However, when the power varied during the surrogate tests, the observed penetration height was not greatly altered (Figure 6.4). As a comparison, the ethylene test, at the conditions stated above, displayed a penetration height of the core of the temperature plume close to 3.0, whereas the surrogate averaged a penetration height close to 7.0. Taking all of the variables into consideration, it appeared that the penetration height was more a function of feedstock than of the power setting or the momentum flux ratio.

Even though the surrogate feedstock had a lower total temperature ratio (approximately 1.25) when compared to the ethylene feedstock (approximately 1.40), the penetration height of the surrogate was much greater. This was a very important observation since one of the purposes of using a plasma torch is to eliminate the need for pyrophoric substances which assists with the spreading of the flame across the combustion region of the scramjet engine. If the penetration height is small, the maximum temperature of the plume remains close to the torch wall and the rest of the combustion chamber has a lower overall temperature. If the penetration height is great enough to spread the plume across the entire combustion chamber of the engine, then there is a possibility of more uniform mixing and combustion since the temperature across the combustion chamber is also more uniform.

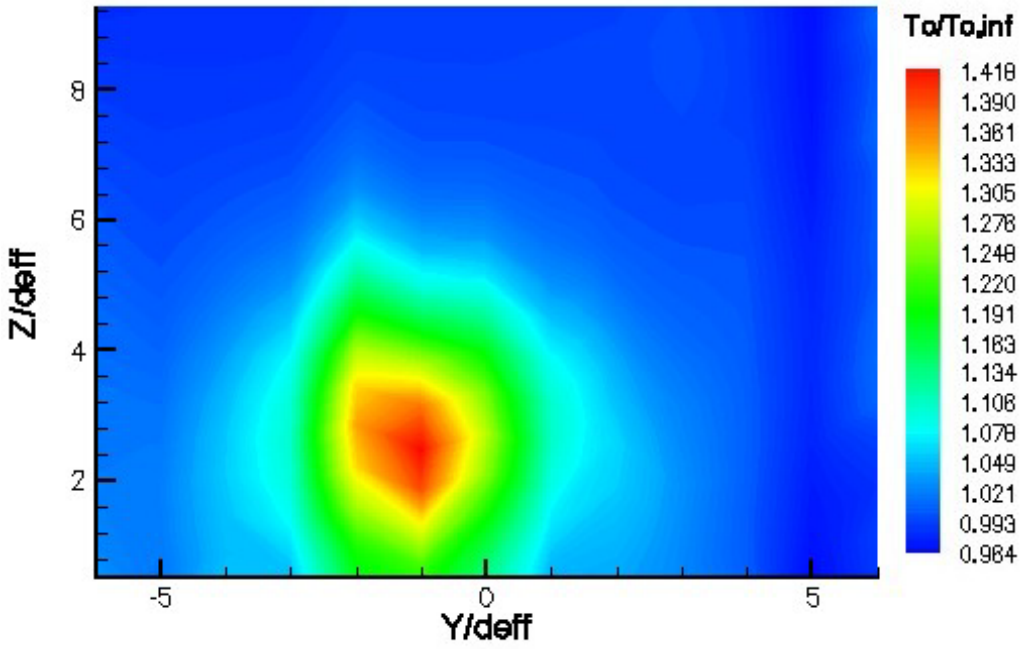

Figure 6.3: Total Temperature Profile of Ethylene at 1500 W [Gallimore 2001]

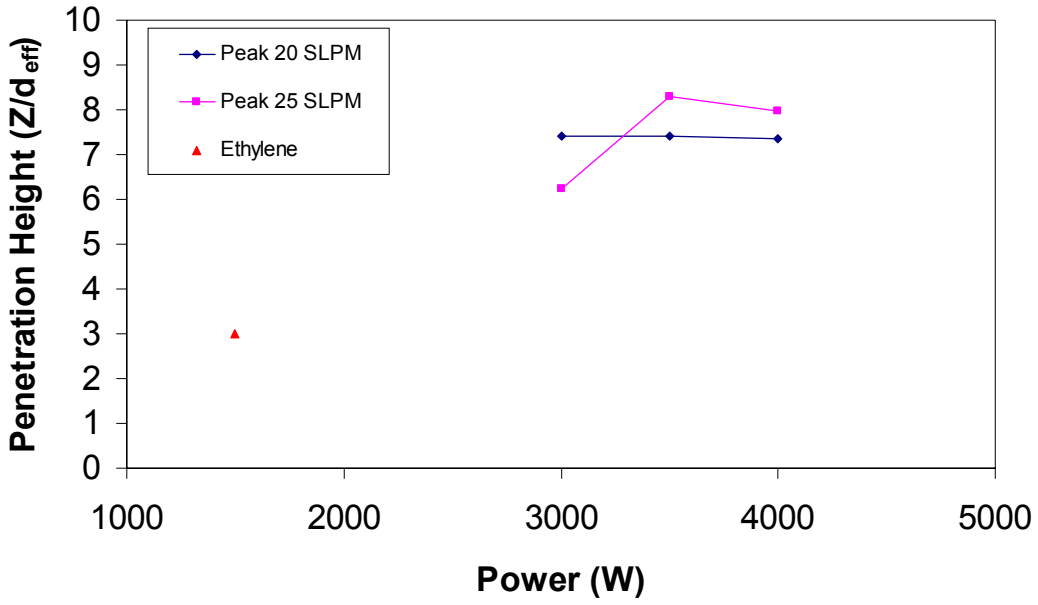

Figure 6.4: Penetration Height of Maximum Core Total Temperature Ratios Taken from Figures 6.1 through 6.3

6.3. Maximum Total Temperature Ratio Comparisons

Another item of interest is the maximum temperature ratio of each profile. Since Figures 6.1 and 6.2 do not encompass the entire total temperature core, it was not an easy task to compare the maximum total temperature ratios of Figures 6.1 and 6.2 to that shown in Figure 6.3. However, the maximum observed temperature ratio of the ethylene at 1.5 kW was 1.418 which, was greater than the maximum temperature ratio of 1.30 of the surrogate at 4.0 kW. If the ethylene feedstock were tested at a comparable power setting to that of the surrogate feedstock, it would be expected to produce a much larger total temperature ratio of the ethylene feedstock than that seen in Figure 6.3. This inconsistency can be attributed to the large amount of energy required to dissociate molecules in the surrogate feedstock compared to the lesser amount of energy required by the ethylene feedstock. Also, since the surrogate feedstock displayed a greater penetration height, there was more opportunity for the surrogate plume to exhibit mixing within the plume which, in turn created a cooling condition for the plume. This cooling

of the plume would directly affect the maximum total temperature ratios recorded during each test run.

6.3.1 Total Temperature Ratio Profiles

Figure 6.5 shows the maximum total temperature ratio plotted against the non-dimensional vertical height through the centerline of the hottest part of the temperature core for an ethylene feedstock gas at various power settings. Figures 6.6 and 6.7 show the same plot but for the surrogate feedstock. The location of the hottest point of the plume can be traced back to the swirling of the plume and erosion of the plasma torch anode. The flow swirler in the chamber of the plasma torch was designed to force the feedstock gas to rotate as it exited the torch. Since the hot gases were always moving in a rotational motion, the arc would be forced to also move in a rotational motion, therefore preventing severe anode erosion. Anode erosion occurs most severely when the arc strikes the same spot on the anode for a prolonged period at a high power setting. As one can see from the total temperature ratio profiles shown in Figures 6.1 through 6.3, there was evidence that the plume was being affected by the swirl and erosion since the hottest location of the plume varied to the left and right of the torch exit.

Due to the location of the total temperature ratio core fluctuating in location between left, center, and right sides of the profiles shown in Figures 6.1 through 6.3, Figures 6.5 through 6.7 were constructed to include the data along the vertical slice that passed through the maximum total temperature ratio of each profile. The plots in Figures 6.6 and 6.7 show the total temperature ratio profile at 3.0, 3.5, and 4.5 kW. Figure 6.6 contains data from runs with a flow rate of 20 SLPM whereas Figure 6.7 contains data from runs with a flow rate of 25 SLPM.

Figures 6.5 through 6.7 show that the maximum total temperature ratio increased as the power increased when the flow rate of the feedstock was held constant. As mentioned earlier, the maximum total temperature ratio of the ethylene was greater than the maximum total temperature ratio of the surrogate thought to be due to mixing and cooling

effects seen by the surrogate feedstock because of the greater penetration height. Dissociation of the molecules in the surrogate feedstock requires more energy than the ethylene feedstock.

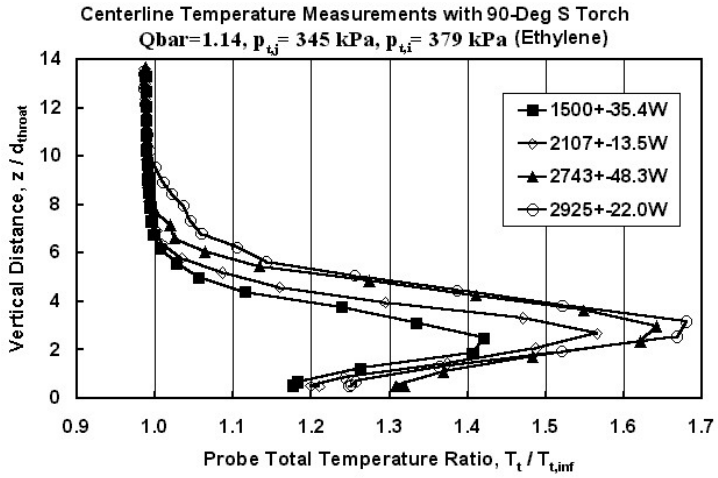

Figure 6.5: Ethylene Centerline Temperature Profiles [Gallimore 2001]

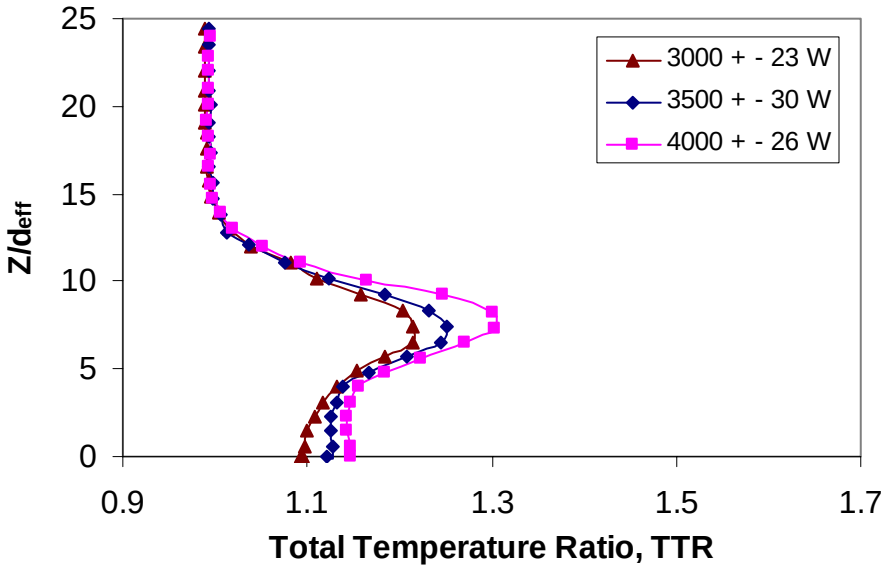

Figure 6.6: Total Temperature Ratio Profile of Surrogate Feedstock at 20 SLPM

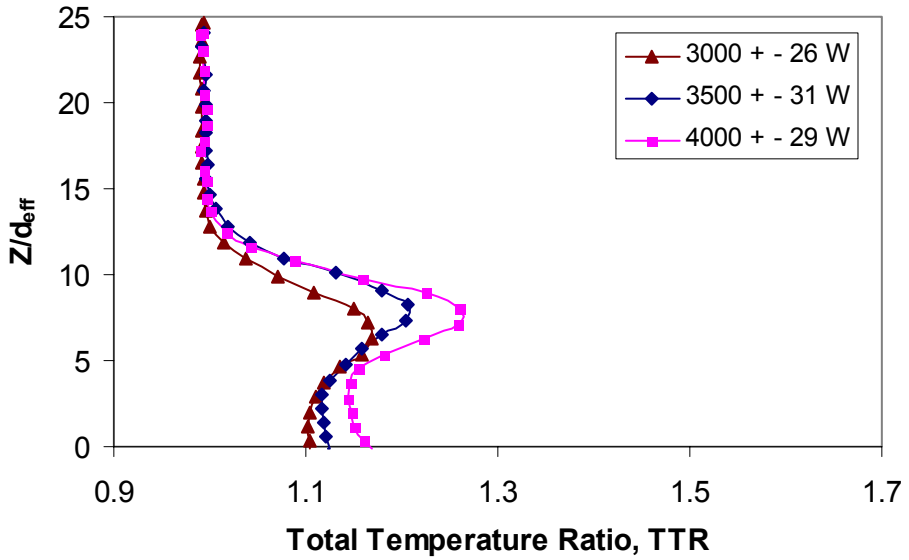

Figure 6.7: Total Temperature Ratio Profile of Surrogate Feedstock at 25 SLPM

6.3.2. Maximum Total Temperature Ratios (Flow rate as a constant)

By plotting the maximum total temperature ratio from each power setting in Figures 6.6 and 6.7, Figure 6.8 was created. Each data set shown in Figure 6.8 held the flow rate constant in order to determine if there were any trends present. For the data set shown, the maximum total temperature ratio increased as the power increased over each flow rate. Work conducted by Gallimore [2001] showed similar trends when methane and ethylene were used as torch feedstocks.

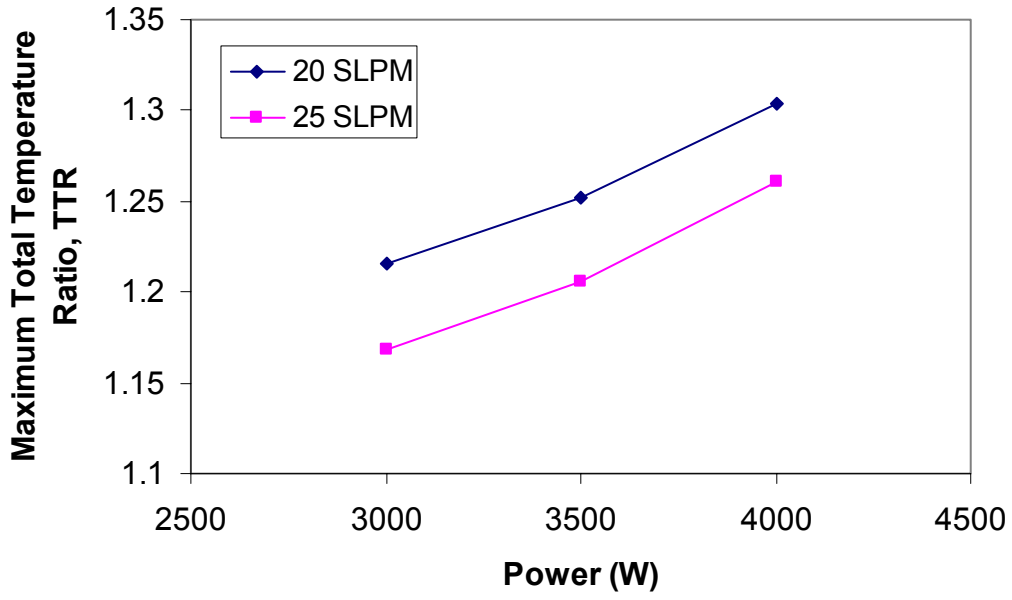

Figure 6.8: The Effect of Increasing Power on Maximum Total Temperature Ratios

6.3.3. Maximum Total Temperature Ratios (Power as a constant)

Using the same data as that in Figure 6.8, Figure 6.9 was generated. This time, holding power constant in order to see how the maximum total temperature ratio varied when the flow rate changed. As the flow rate increased, the maximum total temperature ratio of the core of the plume decreased. Overall, the 25 SLPM flow rate runs displayed a higher penetration height than that of the 20 SLPM flow rate runs. As mentioned previously, as the penetration height of the plume increases, more mixing and cooling could be occurring, which would lower the maximum total temperature ratio.

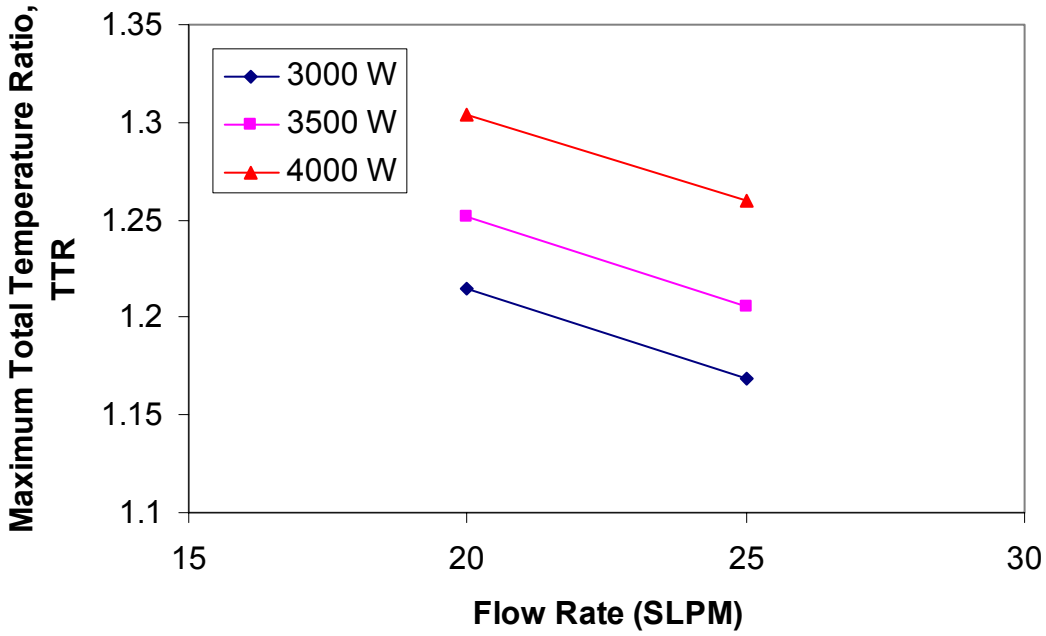

Figure 6.9: The Effect of Fuel Flow Rate on Maximum Total Temperature Ratios

6.4. Total Temperature near the Wind Tunnel Floor

When plotting several of the total temperature profiles (Figures 6.6 through 6.9), the total temperature ratios closest to the floor of the wind tunnel displayed an interesting effect. Figure 6.10 shows how the total temperature ratios varied near the floor (Station Z/d_{eff} = 0). Again, as the power increased for each flow rate, the total temperature ratio increased as expected. However, when comparing the total temperature ratios closest to the floor to the maximum total temperature ratios, the total temperature ratios closest to the floor shows that the higher flow rate has a higher total temperature ratio, whereas the maximum total temperature ratios show that the lower flow rate has a higher total temperature ratio. Since the higher flow rate data displayed a slightly higher penetration height, it experienced slightly more mixing and cooling than the lower flow rate did. The data shown in Figure 6.10 suggests that the plasma torch operates at a somewhat higher total temperature when a higher feedstock flow rate is used. The total temperature data at the test station closest to the floor would be important to know in order to determine how

uniform the total temperature spreads across the combustion chamber for reasons stated in Section 6.2.

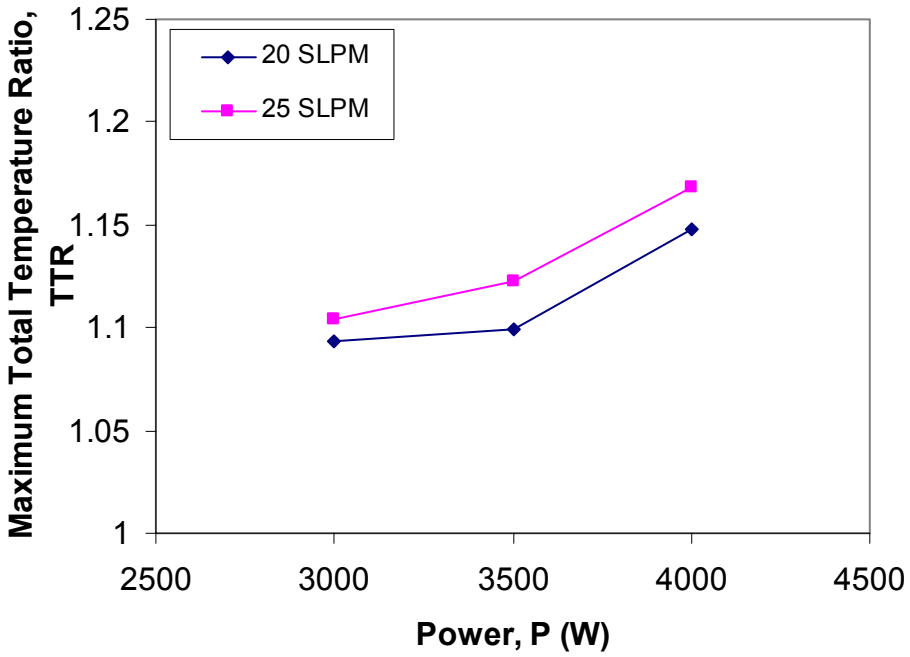

Figure 6.10: Variations in Total Temperature Ratios at Station Closest to the Wind Tunnel Floor

Chapter 7

Conclusions and Recommendations

This chapter will summarize all of the work done and will present the major conclusions drawn from the discussions in previous chapters. Also, recommendations for future work will be made.

7.1. Conclusions

In this study, the 3rd generation Virginia Tech Plasma Torch was used to test a surrogate feedstock gas of thermally-cracked JP-7, which consisted of 15 % methane, 25 % ethane, and 60 % ethylene, by volume. The torch was first tested in a quiescent test cell to collect spectrograms of the plume generated by the surrogate feedstock gas. The torch was also testing in a Mach 2.4 cross flow in the Virginia Tech Supersonic Wind Tunnel where total temperature data were collected 7.6 cm downstream of the torch exit. Flow rates of 20 and 25 SLPM and power settings of 3.0, 3.5, and 4.0 kW were used in the tests.

Upon inspection of the spectrograms taken at various power settings, the species present within the plume are found to be the same as the species found in spectrograms of methane and ethylene. The relative intensities of each specie varied due to variations in the reaction mechanisms since the surrogate feedstock gas is different than pure methane or pure ethylene. Important species that appeared in the spectrograms include CN, C, C_2, CH, H_2, and H, which can interact freely with other molecules to enhance combustion. There was no evidence of OH radicals within the spectrograms, which is a dominant radical representing combustion. The majority of the spectroscopic data were collected in the quiescent test cell. The spectroscopic analysis was not duplicated in full in the

supersonic environment since the spectroscopic data collected in the supersonic wind tunnel produced similar results to the quiescent environment.

Upon inspection of several still photographs (Figure 5.7) taken of the plume during a single test run in the supersonic wind tunnel, it was observed that the plume was oscillating. Previous work [Gallimore 2001] indicated that plasma torch oscillations originated from 3-phase, unfiltered, rectified power. These oscillations at 180 Hz were the source of the oscillations in the plume itself. Since the images presented in Chapter 5 were taken manually on a digital camera, there was no way to verify the frequency at which the plume was oscillating. Since the shutter speed was set to 1/500 sec and the oscillations are thought to be at 180 Hz, the individual images would not be blurred by these oscillations.

Without changing any variables on the spectrometer set-up, three data sets were taken to observe how the power variations may affect the intensities of the species within the spectrogram of the plasma plume. Work completed by Gallimore [2001] found that as the power increases, the intensities of the species will increase. Figure 5.12 shows that as the power increases, the intensities of a random sample of species also increase, confirming the findings of the previous work.

Keeping in mind how the intensities could vary, spectroscopic data were collected at various locations in the plume. It was found that at the torch exit, where the core of the aureole is located, the intensities of all the species were very well defined and were more luminescent. The further from this point, the weaker the intensities become, but the species present remain the same. Due to the pace at which the relative intensities decrease from the 0 mm location to the 4.125 mm location (discussed in Appendix B), it can be concluded that the edge of the aureole lies within this region.

The analysis of the spectrograms collected from both the quiescent environment and the supersonic environment showed that the species generated in each condition were the same. Due to the differences in the environment, the intensities of similar peaks varied.

This can be attributed to the quenching effect which commonly occurs in a supersonic environment. Otherwise, the quiescent environment provides a sufficient test bed in terms of identifying the species present in the plasma torch plume.

The molybdenum anode and tungsten cathode experienced erosion during testing. In past Virginia Tech plasma torch tests, the electrodes lasted for many runs (several hours) [Stouffer 1989]. The electrodes used for this work lasted for approximately ten runs on average, which is equivalent to a few minutes. Higher power settings as well as poorly aligned electrodes appeared to cut the life of the electrodes considerably.

Considering the total temperature data collected in the supersonic wind tunnel, the first conclusion to discuss is that of the plume penetration height based on the maximum total temperature ratio. When looking at just the surrogate total temperature ratio profiles (Figure 6.4), one can see that the penetration height does not fluctuate much when the power or the flow rate increases, which suggests that the power setting does not affect the penetration height of the maximum total temperature ratio of the plume. When comparing the total temperature ratio profiles of the surrogate feedstock to that of the ethylene feedstock, the difference in penetration heights of the maximum total temperature ratio is quite significant. The surrogate feedstock has a penetration height about twice that of the ethylene feedstock, which is a considerable finding since greater penetration may equate to greater ignition potential and could lead to the replacement of pyrophoric substances currently being used.

When the flow rate was held constant and the torch power increased, the overall maximum total temperature ratio increased. This was expected since there would be more energy to interact with the molecules and the remaining energy would, in turn, heat the emissions from the torch. However, when holding the power constant and varying the fuel flow rate, the maximum total temperature ratio decreased. Also, when comparing the maximum total temperature of the surrogate to that of the ethylene data, the surrogate displayed a much lower maximum total temperature. The lower total temperature ratio in the surrogate can be attributed to the added amounts of mixing and

therefore cooling of the plume due to the higher penetration height when compared to the ethylene data in similar supersonic environments.

Finally, the data collection station located nearest to the floor of the wind tunnel displayed an interesting effect. As the power increased, so did the maximum total temperature at that station. This effect occurred for both flow rates presented and can be attributed to the boundary layer trapping the hot gases close to the wind tunnel floor.

7.2. Recommendations for Future Work

With a project as encompassing as this research, more data is required to fully understand all of the intricate details. The work presented here is just the beginning of a much larger project that will enable us to understand how a plasma torch operates with a JP-7 feedstock (gaseous and liquid) in various states. In order to determine the trends that occurred, more data needs to be collected to better quantify the trends discussed in this thesis.

A study of the floor heating phenomenon should be considered to determine if there is a way to enhance the spreading of the plume. Spreading of the hot gases of the plasma torch can enhance combustion and may warrant the removal of other combustion enhancing aids.

More testing needs to be completed in order to fully understand the oscillatory behavior of the plume. It has been discovered that the oscillations seen in the plume occur due to oscillations within the power supplied to the torch. If these oscillations can be controlled, it may be possible to use the oscillations to our advantage in allowing the torch to operate more efficiently.

After all of the data were collected for this work, it was found that the alignment of the electrodes may have been the cause of the shortened life span of the electrodes. Even

though great care was taken in order to align the electrodes properly, recent discussions suggest that the alignment was not adequate. Before more data is collected using this generation plasma torch, a new alignment method should be developed to ensure proper alignment of the electrodes which, in turn, will allow a longer-lived plasma torch. Also, a new power connection method needs to be developed for the quiescent test cell to prevent an arc-current magnetic field on the arc which may cause some erosion.

Another suggestion for future work would be to incorporate the gaseous surrogate feedstock operated torch with an aeroramp injector located upstream of the torch in order to determine if the plasma plume penetration and ignition potential improves with additional fuel. Previous work has shown that the plasma torch, in conjunction with an aeroramp injector, improved operational characteristics, such as plume penetration, than the plasma torch alone [Gallimore 2001]. Combinations of various aeroramp feedstocks in conjunction with the gaseous surrogate operated plasma torch should be tested.

Finally, the plasma torch should be tested with a liquid JP-7 fuel. Although at advanced stages of flight a gaseous cracked JP-7 fuel is available, at the start of flight only liquid fuel is available. If the plasma torch can be proven to work on liquid JP-7 in addition to the gaseous cracked JP-7, the applications for a plasma torch would multiply greatly.

References

1) Andrews, Earl H., "Scramjet Development and Testing in the United States," 10th International Space Planes and Hypersonic Systems and Technologies Conference, AIAA 2001-1927, April 2001.

2) Andrews, Earl H.; Torrence, Marvin G.; Anderson, Griffin Y.; Northam, G. B.; Mackley, Ernest A., "Langley Mach 4 Scramjet Test Facility," NASA TM 86277, February 1985.

3) Andrews, Earl H, "A Subsonic to Mach 5.5 Subscale Engine Test Facility," AIAA 87-2052, 1987.

4) Barbi, E., "Uncooled Choked Plasma Torch for Ignition and Flameholding in Supersonic Combustion," Masters Thesis, Virginia Polytechnic Institute and State University, 1986.

5) Barbi, E., Mahan, J.R., O'Brien, W.F. and Wagner, T.C., "Operating Characteristics of a Hydrogen-Argon Plasma Torch for Supersonic Combustion Applications," Journal of Propulsion, Vol. 5, No. 2, pp. 129-133, 1989.

6) Cobine, James Dillon, "Gaseous Conductors Theory and Engineering Applications," Dover Publications, New York, 1958.

7) Curran, Edward T., "Scramjet Engines: The First Forty Years;" Journal of Propulsion and Power, Vol. 17, No. 6, November – December 2001.

8) Dornheim, Michael A., "X-43 Flight Test Indicates Thrust is Greater Than Drag," Aviation Week & Space Technology, McGraw-Hill Company, April 2004.

9) Ferri, A., "Discussion on M. Roy's Paper Propulsion Supersonique par Turboreacteurs et par Statoreacteurs," Advances in Aeronautical Sciences, Vol. 1, Pergamon, pp. 79-112, 1959.

10) Ferri, A., Libby, P.A. and Zakkay, V., "Theoretical and Experimental Investigations of Supersonic Combustion," Proceedings of the International Council of the Aeronautical Sciences, Third Congress, Stockholm, 1962, Spartan, New York, pp 1089-1155, 1964.

11) Gallimore, S.D., "Development and Operating Characteristics of an Improved Plasma Torch for Supersonic Combustion Applications," Masters Thesis, Virginia Polytechnic Institute and State University, 1998.

12) Gallimore, S.D., "A Study of Plasma Ignition Enhancement for Aeroramp Injectors in Supersonic Combustion Applications," Ph.D. Dissertation, Virginia Tech, May 2001.

13) Gallimore, S.D., Jacobsen, L.S., O'Brien, W.F. and Schetz, J.A., "An Integrated Aeroramp-Injector/Plasma Ignitor for Hydrocarbon Fuels in Supersonic Flow," 10th International Space Planes and Hypersonic Systems and Technologies Conference, AIAA 2001-1767, April 2001.

14) Gallimore, S.D., Jacobsen, L.S., O'Brien, W.F. and Schetz, J.A., "Spectroscopic Investigations of Hydrocarbon- and Nitrogen-Based Plasmas for Supersonic Ignition," 11th International Space Planes and Hypersonic Systems and Technologies Conference, AIAA 2002-5247, October 2002.

15) Gallimore, S.D., Jacobsen, L.S., O'Brien, W.F. and Schetz, J.A., "Operational Sensitivities of an Integrated Scramjet Ignition/Fuel-Injection System," Journal of Propulsion and Power, Vol.19, No. 2, pp. 183-189, 2003

16) Gaydon, A.G., The Spectroscopy of Flames, 2nd Ed., Chapman and Hall, London, pp.99-144, 1974.

17) Guy, Robert W, Torrence, Marvin G., Sabol, Alexander P. and Mueller, James N., "Operating Characteristics of the Langley Mach 7 Scramjet Test Facility," NASA TM 81929, 1981.

18) Harrison, A.J. and Weinberg, F.J., "Flame Stabilization by Plasma Jets," Proceedings of the Royal Society of London, Vol. 321, pp. 95-103, 1971.

19) http://nix.nasa.gov, February 13, 2004.

20) http://www.aviation-history.com, Feb. 3, 2004.

21) Jacobsen, L.S., Gallimore, S.D., Schetz, J.A., O'Brien, W.F. and Goss, L.P., "An Improved Aerodynamic Ramp Injector in Supersonic Flow," 39th Aerospace Sciences Meeting and Exhibit, AIAA 2001-0518, January 2001.

22) Jacobsen, Lance S., Carter, Campbell D., Baurle, Robert A. and Jackson, Thomas A., "Toward Plasma-Assisted Ignition for Scramjets," 41st Aerospace Sciences Meeting and Exhibit, AIAA 2003-0871, January 2003.

23) Jacobsen, L. S., Gallimore, S.D., Schetz, J.A., O'Brien, W.F., "Integration of an Aeroramp Injector/Plasma Igniter for Hydrocarbon Scramjets," Journal of Propulsion and Power, Vol. 19, No. 2, pp. 170-182, 2003.

24) Kelly, Michael, news@afrl Features; October 2002.

25) Kimura, Itsuro, Aoki, Hiroshi and Kato, Manabu, "The Use of a Plasma Jet for Flame Stabilization and Promotion of Combustion in Supersonic Air Flows," Combustion and Flame, Vol. 42, pp 297-305, 1981.

26) Kitagawa, Tomoaki, Moriwaki, Atsushi, Takita, Kenichi and Masuya, Goro, "Ignition Characteristics of Methane and Hydrogen Using a Plasma Torch in Supersonic Flow," Journal of Propulsion and Power, Vol. 19, No. 5, pp. 853-858, 2003.

27) Kuo, S.P., Bivolaru, Daniel, Carter, Campbell D., Jacobsen, Lance and Williams Skip, "Operational Characteristics of a Plasma Torch in a Supersonic Cross Flow," 41st Aerospace Science Meeting and Exhibit, AIAA 2003-1190, January 2003.

28) Lawton, J. and Weinberg, F.J., "Electrical Aspects of Combustion," Clarendon Press, 1969.

29) Masuya, G., Sayama, M., Ohwaki, K. and Kimura, I., "Some Governing Parameters of Plasma Torch Igniter/Flameholder in a Scramjet Combustor," Journal of Propulsion and Power, Vol. 9, No. 2, March 1993.

30) Moses, Paul L., "X-34C Plans and Status," 12th International Space Planes and Hypersonic Systems and Technologies Conference, AIAA 2003-7084, December 2003.

31) Mozingo, Joseph A., "Evaluation of a Strut-Plasma Torch Combination as a Supersonic Igniter-Flameholder," Masters Thesis, Virginia Polytechnic Institute and State University, March 2004.

32) Northam, G. Burton, McClinton, Charles R., Wagner, Timothy C. and O'Brien, W.F., "Development and Evaluation of a Plasma Jet Flameholder for Scramjets," 20th Joint Propulsion Conference, AIAA 84-1408, 1984.

33) Orrin, J.E., Vince, I.M. and Weinberg, F.J., "A Study of Plasma Jet Ignition Mechanisms," 18th Symposium on Combustion, The Combustion Institute, pp 1755-1765, 1981.

34) Pearse, R.W.B. and Gaydon, A.G., The Identification of Molecular Spectra, 4th Ed., Chapman and Hall, London, pp. 82-86, 103-6, 169-170, 255-9, 264-5, 388-391, 1976.

35) Rock, Kenneth E., Andrews, Earl H. and Eggers, James M., "Enhanced Capability of the Combustion Heated Scramjet Test Facility," AIAA 91-2502, June 1991.

36) Shuzenji, Kiyotaka, Kato, Ryoichi and Tachibana, Takeshi, "Two-Stage Plasma Torch Ignition in Supersonic Airflows," 37th Joint Propulsion Conference, AIAA 2001-3740, July 2001.

37) Stouffer, Scott, "Development an Operating Characteristics of an Improved Plasma Torch for Supersonic Combustion Applications," Masters Thesis, Virginia Polytechnic Institute and State University, July 1989.

38) Takita, K., Sato, T., Ju, Y. and Masuya, G., "Effects of Addition of Radicals Supplied by Plasma Torch on Burning Velocity," 35th Joint Propulsion Conference, AIAA 99-2247, June 1999.

39) Thomas, Scott R. and Guy, Robert W., "Increased Capabilities of the Langley Mach 7 Scramjet Test Facility," AIAA 82-1240, June 1982.

40) Wagner, T.C., "Ignition and Flameholding in Supersonic Flow by Injection of Dissociated Hydrogen," Ph.D. Dissertation, Virginia Polytechnic Institute and State University, February 1987.

41) Wagner, Timothy C., O'Brien, Walter F., Northam, G. Burton and Eggers, James M., "Plasma Torch Igniter for Scramjets," Journal of Propulsion and Power, Vol. 5, No. 5, pp. 548-554, September – October 1989.

42) Waltrup, P.J., "Hypersonic Airbreathing Engines: Evolutions and Opportunities," AGARD CP-428, Paper 12, April 1987.

43) Waltrup, P.J., White, M.E., Zarlingo, F. and Gravelin, E.S., "History of U.S. Navy Ramjet, Scramjet, and Mixed-Cycle Propulsion Development," 32nd Joint Propulsion Conference and Exhibit, AIAA 96-3152, July 1996.

44) Waltrup, Paul J., Anderson, Griffin Y. and Stull, Frank D., "Supersonic Combustion Ramjet (Scramjet) Engine Development in the United Sates," Proceedings – 3rd International Symposium on Air Breathing Engines, Dietmar K. Hennecks and Gert Winterfeld, eds. DFLR Fachbuchreihe Bd.6, pp. 835-861, 1976.

45) Waltrup, Paul J.,"Upper Bounds on the Flight Speed of Hydrocarbon-Fueled Scramjet-Powered Vehicles," Journal of Propulsion and Power, Vol. 16, No. 6, pp.1199-1204, 2001.

46) Warris, A.M. and Weinberg, F.J., "Ignition and Flame Stabilization by Plasma Jets in Fast Gas Streams," 20th Symposium of Combustion, The Combustion Institute, pp. 1825-1831, 1984.

47) Weinberg, F.J., "Old Flames and New," Inaugural Lectures, Imperial College, 1968.

48) Weinberg, F.J., Hom, K., Oppenheim, A.K. and Teicham, K., "Ignition by Plasma Jet," Nature, Vol. 272, pp 341-343, 1978

49) Williams, Robert M., "National Aerospace Plane: Technology for America's Future," Aerospace America, pp. 18-22, November 1986.

50) Zelina, J. and Ballal, D.R., "Combustion and Emissions Studies Using a Well Stirred Reactor," 30th Joint Propulsion Conference, AIAA 94-2903, June 1994.

51) Zelina, J.; Wright Patterson Air Force Base; personal conversations; October 2002.

Appendix A

Development of the Virginia Tech Plasma Torch

Over the years, there have been several plasma torches developed at Virginia Tech. In the mid-80s, Wagner began testing a plasma torch for supersonic combustion applications. He began his work with a commercial, water-cooled torch from Plasmadyne shown in Figure A.1. It contained a tangential feedstock gas inlet which was used to induce swirl in the chamber of the torch and therefore to increase the life of the anode. Wagner attempted to run the torch on such fuels as hydrogen, argon, nitrogen and mixtures of argon with either nitrogen or hydrogen. This torch did not perform as well as one would have liked due to the torch exit not being choked, which allowed pressure fluctuations outside of the torch to influence the stability of the arc. This caused the torch to blow out with changes in the wind tunnel operation and even with changes in the ignition of the fuel. To compensate for this problem, a new torch was needed and Barbi developed what is now known as Virginia Tech Plasma Torch 1 (VTPT-1).

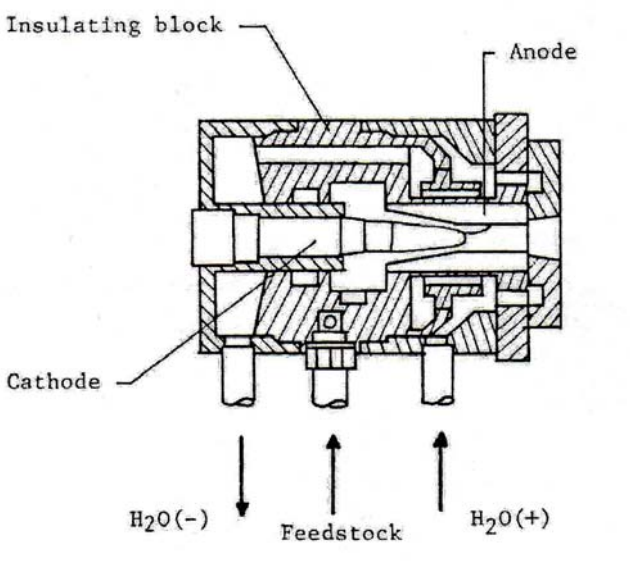

Figure A.1: Section Drawing of Plasmadyne Torch [Wagner 1987]

Based on the design issues of the Plasmadyne torch, Barbi developed VTPT-1 which contained a choked exit (see Figure A.2). This would allow the torch to operate even with the fluctuations of the wind tunnel or the variations of ignition parameters outside of the torch. It was also designed to operate on very low powers (between 0.5 – 2 kW) and on similar gases as that of the Plasmadyne torch. The design of the VTPT-1 was similar to the Plasmadyne torch such that it also contained a tangential feedstock inlet to induce flow swirling within the chamber of the torch body which reduced the erosion of the anode. VTPT-1 was designed as an uncooled torch and therefore did not need the water cooling channels. All of the heat that the water cooling carried away in the Plasmadyne torch was now being carried away by the feedstock gas out of the exit of the torch. The energy provided by the excess heat was now added to the cross stream flow making this new torch design more efficient. The thermal efficiency, defined as the ratio of total enthalpy of the gas exiting the torch versus the electrical power input, was calculated to be 88%.

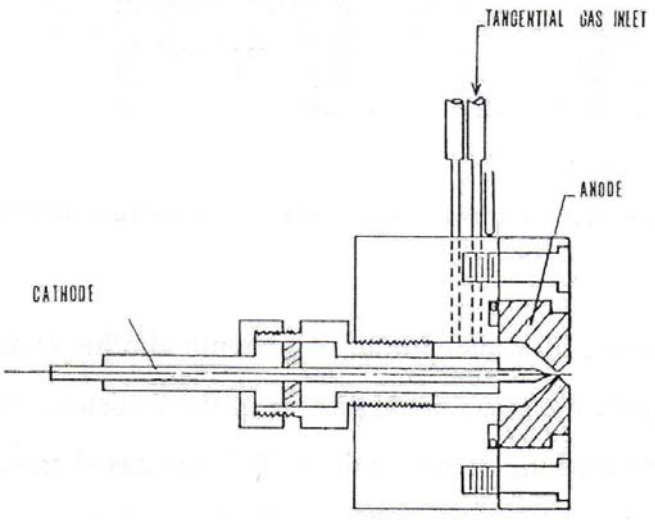

Figure A.2: VTPT-1 Section Drawing [Barbi 1986]

Although VTPT-1 was an improvement over the original torch tested at Virginia Tech, a new torch was developed by Stouffer that had a much longer lifetime than the previous designs.VTPT-2, shown in Figure A.3 included new features such as a flow swirler, an

electrode alignment system, and an adjustable electrode gap feature. The flow swirler allowed the feedstock gas to be introduced to the torch without having to deal with orientation of the feedstock line. The electrode alignment system allowed the electrodes to be aligned much more easily than before and therefore helped extend the lifetime of the electrodes. The last feature allowed the gap to be adjusted and allow the torch to be operated on the same power setting as previous runs. This torch was operated on feedstocks such as nitrogen, argon and mixtures of argon with either hydrogen or nitrogen. With the new features, this torch has been shown to operate for more than twenty hours when the feedstock gas was a mixture of argon and nitrogen.

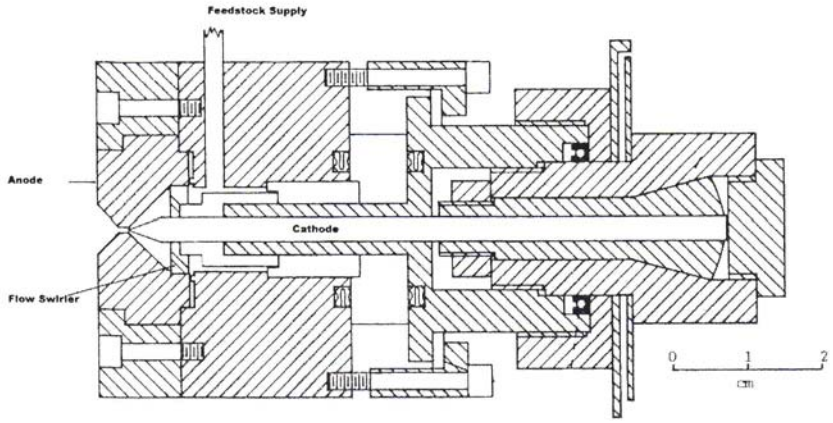

Figure A.3: VTPT-2 Section Drawing [Stouffer 1989]

Gallimore [1998] began his work with VTPT-2 by running the torch on light hydrocarbon feedstock gases such as methane, propane and ethylene. He found that as the chain length of the hydrocarbons increased, the required power to stabilize the torch also increased.

Gallimore [2001] and Jacobsen [2001] began to work on integrating the plasma torch with an aeroramp and required a slightly smaller torch to allow room for the aeroramp. VTPT-3, seen in Figure A.4, was developed for this integrated work and proved to have several benefits over VTPT-2 such as having fewer parts to machine, greater sealing abilities and allowing the electrodes to be replaced in less time. VTPT-3 has some similarities to VTPT-2 such as the choked exit, utilizing a flow swirler, and not requiring

cooling. Gallimore's work with VTPT-3 included torch feedstock gases such as argon, nitrogen, air, methane, and ethylene. He ran the torch on powers ranging from 0.5 to 4kW. Gallimore also conducted a survey of various anode geometries and found that the anode (A) shown in Figure A.4 was the optimal anode for supersonic applications. VTPT-3 is used in the current work and an in depth discussion about it can be found in Chapter 2.

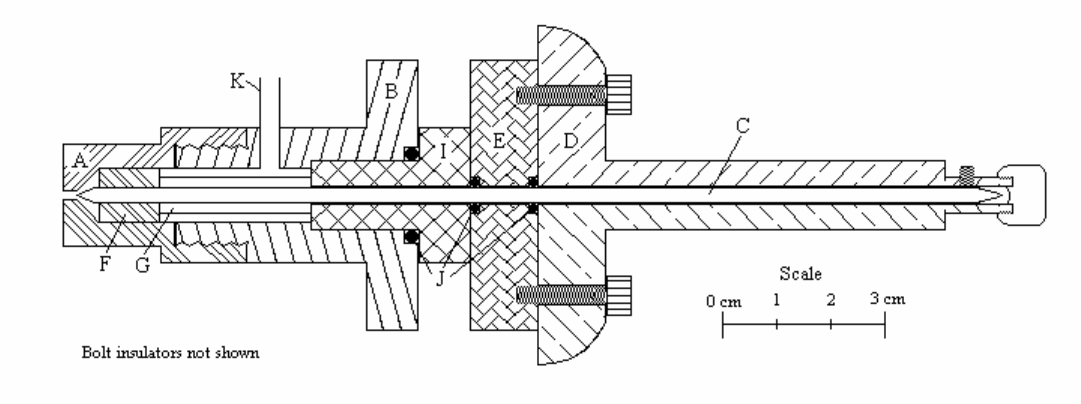

Figure A.4: VTPT-3 Section Drawing [Gallimore 2001]

VTPT-3 was also used in the work conducted by Mozingo [2004]. Mozingo used the torch as an igniter and flameholder at the base of a strut injector. He operated the torch at powers from 1.5- to 2.5-kW on a feedstock of nitrogen.

The combined work of Gallimore and Jacobsen led to the design of VTPT-4, seen in Figure A.5. It contains all of the features of VTPT-3 but requires less volume. One difference between the two torches is that VTPT-4 utilized anode inserts (11 in Figure A.5) which are easier to machine and cost effective. This torch was intended to be used in a heated supersonic combustion wind tunnel at Wright Patterson Air Force Base in Dayton, OH.

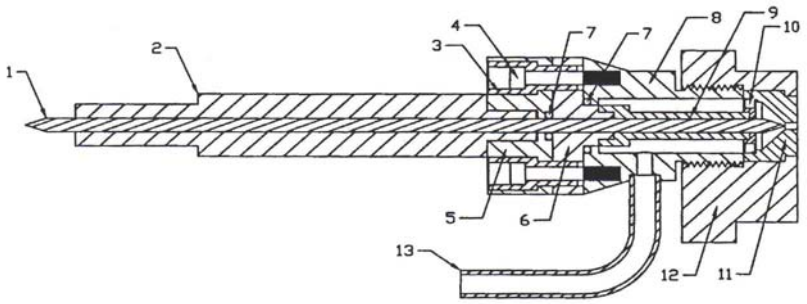

Figure A.5: VTPT-4 Section Drawing [Jacobsen 2001]

Cooperative work between Gallimore and Mozingo led to the development of another torch, known as VTPT-5. Due to its extremely small size, an anode tip was used as opposed to a full anode like the other torches described in this section, see Figure A.6. This torch was designed for reduced drag experiments at the Arnold Engineering Development Center (AEDC).

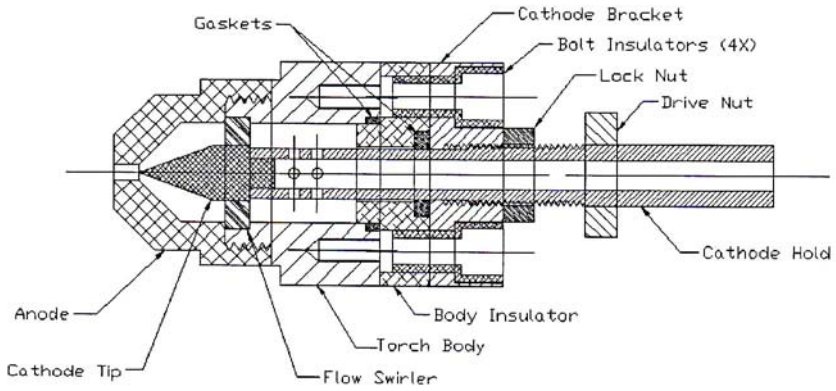

Figure A.6: VTPT-5 Section Drawing [Mozingo 2004]

Virginia Tech has worked on plasma torch development over many years, and has made many significant improvements to plasma torch technology. The current work is part of a larger program to use a plasma torch with a liquid feedstock and, as a result, a new torch is expected to be developed from the program. The current work is just the first step in this new program and therefore utilized the current technology of VTPT-3.

Appendix B

Study of How Intensities Varies within the Plume

This appendix is a continuation of Section 5.3. The spectrometer integration time was set to 40 ms and the spectrometer was traversed in the configuration shown in Figure B.1 for both quiescent and supersonic runs presented here. Starting at the torch exit, eight sampling stations every 4.125 mm were used to collect the spectroscopic data. Since the spectroscopic data beyond 12.375 mm appeared no different than noise in the signal, only data from 0 (sampling station 1 in Figure B.1) through 12.375 (sampling station 4 in Figure B.1) mm will be presented. Figures B.2 through B.5 show data collected in the quiescent environment when the torch was operated at 3.0 kW. Figures B.6 through B.9 show data collected in the supersonic environment when the torch was operated at 4.0 kW.

Figures B.10 through B.12 show the variations in intensity for peaks at various wavelengths as the data collection station moved away from the torch exit. Figure B.10 shows all of the quiescent data, Figure B.11 shows all of the supersonic data, and Figure B.12 shows both quiescent and supersonic data together. In discussions made by Cobine [1958], he said that the core of the aureole is a region of intense chemical activity where there is a high temperature that all gases are largely dissociated. Beyond this intense region, the chemical activity and high temperatures drop significantly. If the chemical

activity and temperatures drop quickly, then the luminosity would be expected to decrease as well. There is a large drop in intensity between torch exit and 4.125 mm away from torch exit. Once beyond the core of the aureole, there is little difference in the rate at which relative intensity decreases. As one can see from Figure B.10, the further from the core of the aureole data is collected, the lower the relative intensities become. It can be inferred from this definition that the edge of the aureole region is located between 0 and 4.125 mm. The data collected for the series representing 652.3 nm in the supersonic environment appears to be outlier data due to the fact that it does not follow the same trends as the other series shown in Figure B.10.

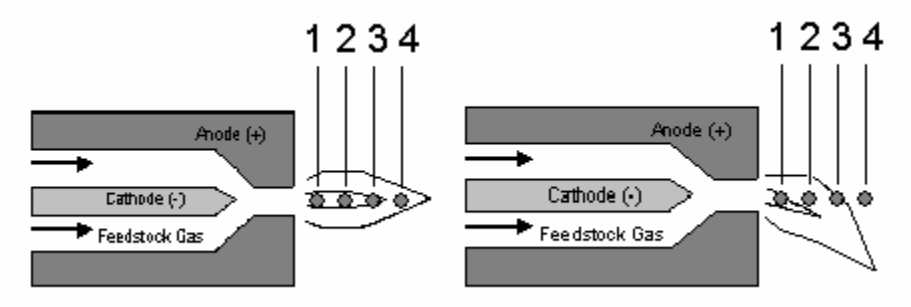

(A) (B)

Figure B.1: Sampling Stations Used to Collect Spectrometer Data in Quiescent (A) and Supersonic (B) Environments

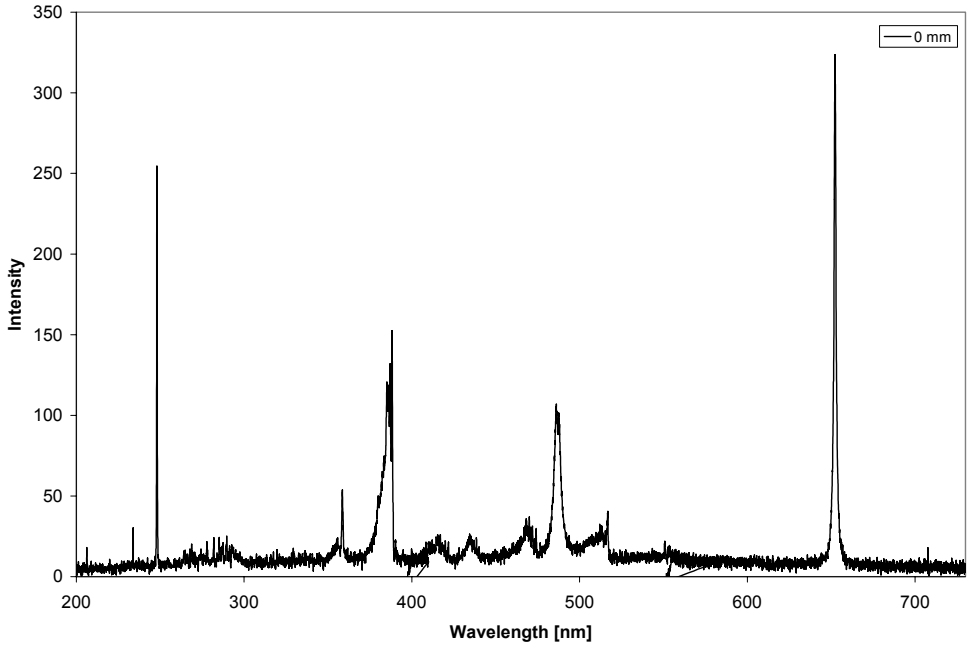

Figure B.2: Spectroscopic Data Collected in the Quiescent Environment with the Torch Operating at 30 SLPM, 3.0 kW, and the Spectrometer Integration Time Set to 40 ms at Station 1

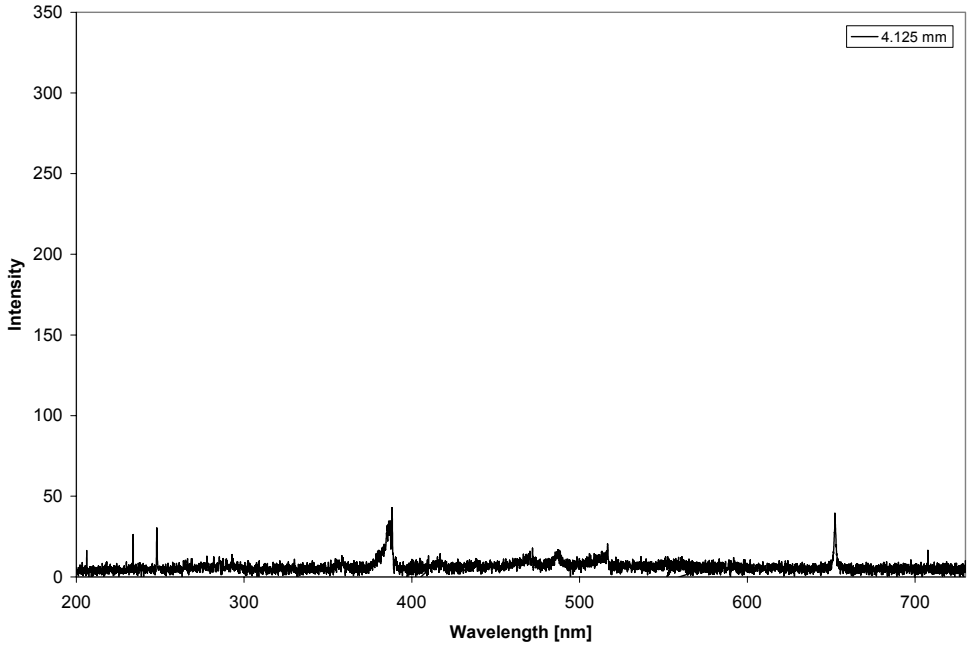

Figure B.3: Spectroscopic Data Collected in the Quiescent Environment with the Torch Operating at 30 SLPM, 3.0 kW, and the Spectrometer Integration Time Set to 40 ms at Station 2

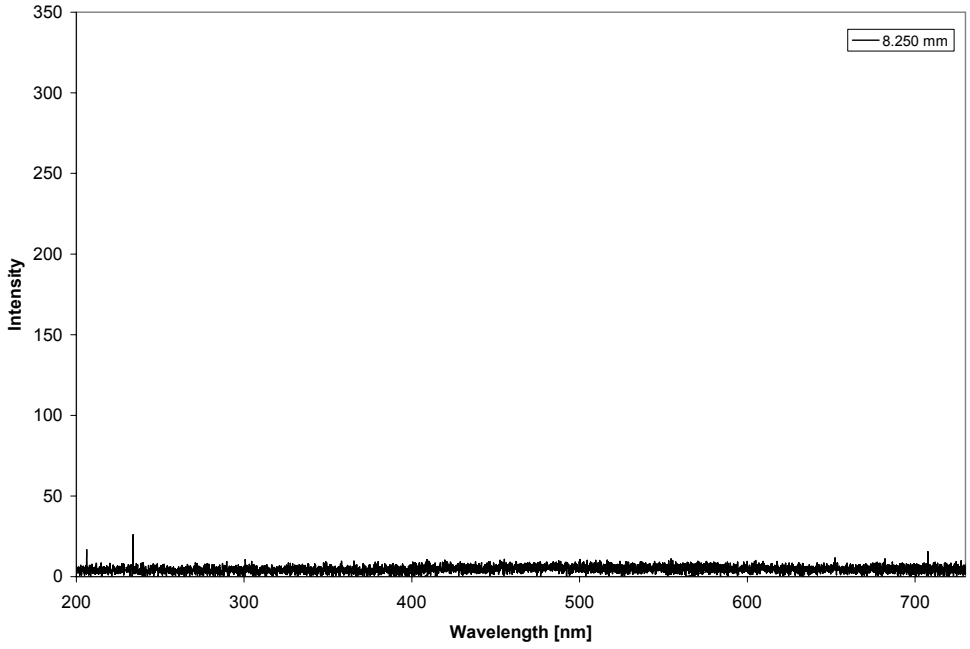

Figure B.4: Spectroscopic Data Collected in the Quiescent Environment with the Torch Operating at 30 SLPM, 3.0 kW, and the Spectrometer Integration Time Set to 40 ms at Station 3

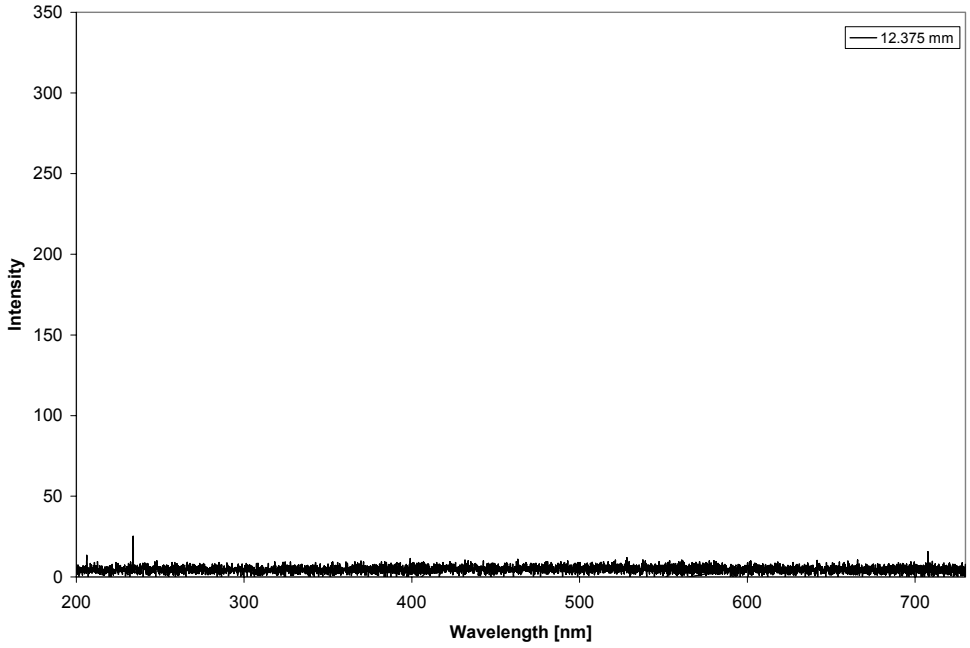

Figure B.5: Spectroscopic Data Collected in the Quiescent Environment with the Torch Operating at 30 SLPM, 3.0 kW, and the Spectrometer Integration Time Set to 40 ms at Station 4

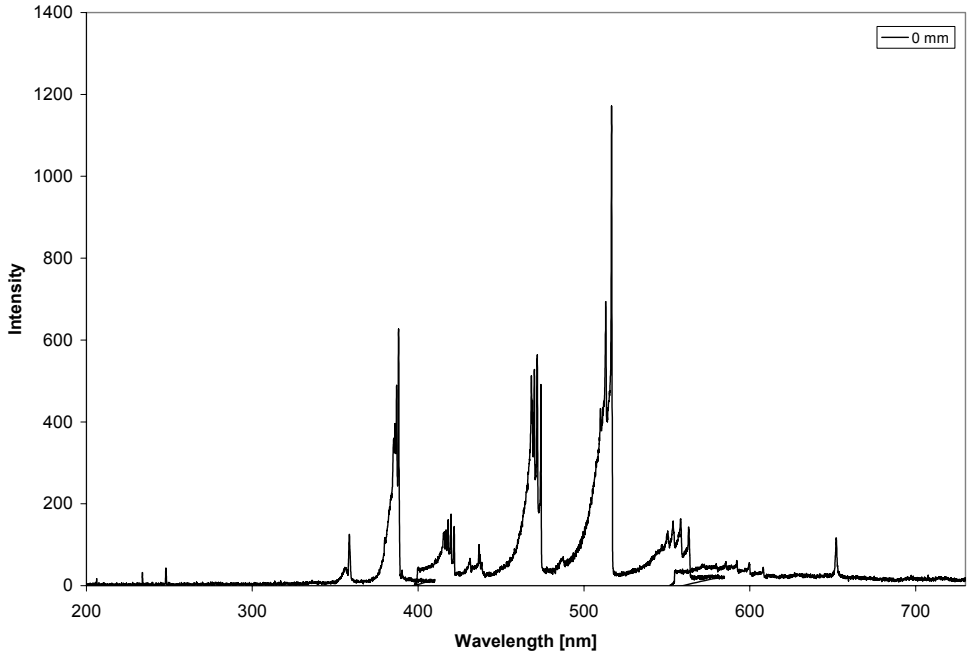

Figure B.6: Spectroscopic Data Collected in the Supersonic Environment with the Torch Operating at 30 SLPM, 4.0 kW, and the Spectrometer Integration Time Set to 40 ms at Station 1

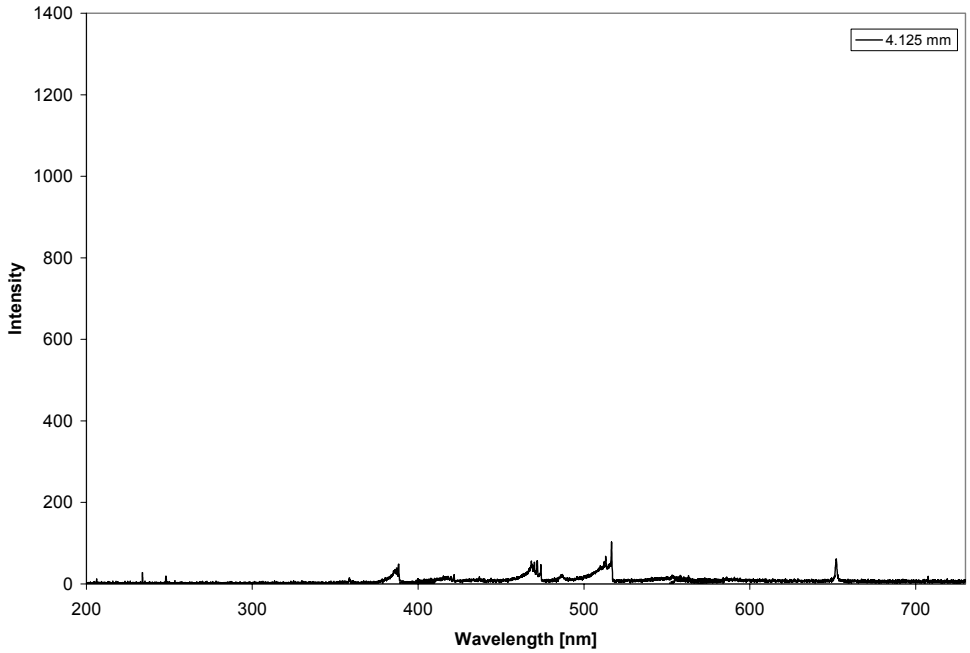

Figure B.7: Spectroscopic Data Collected in the Supersonic Environment with the Torch Operating at 30 SLPM, 4.0 kW, and the Spectrometer Integration Time Set to 40 ms at Station 2

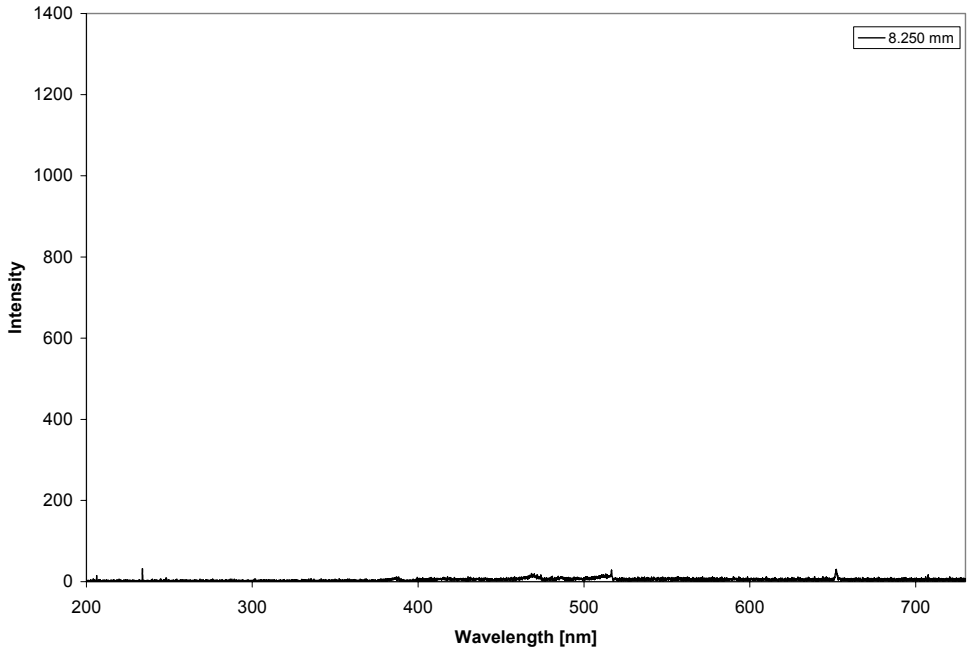

Figure B.8: Spectroscopic Data Collected in the Supersonic Environment with the Torch Operating at 30 SLPM, 4.0 kW, and the Spectrometer Integration Time Set to 40 ms at Station 3

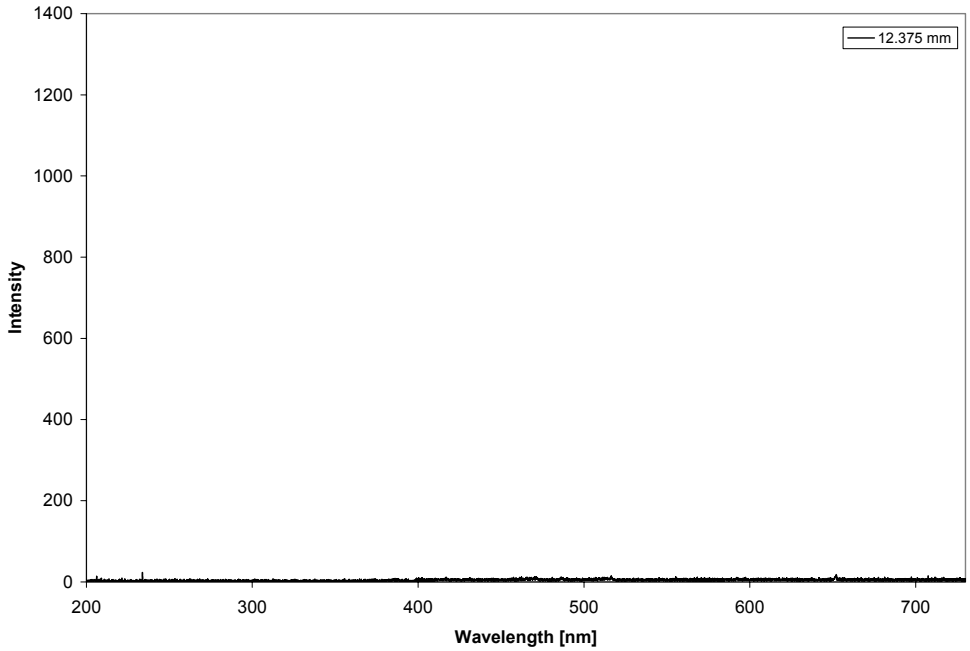

Figure B.9: Spectroscopic Data Collected in the Supersonic Environment with the Torch Operating at 30 SLPM, 4.0 kW, and the Spectrometer Integration Time Set to 40 ms at Station 4

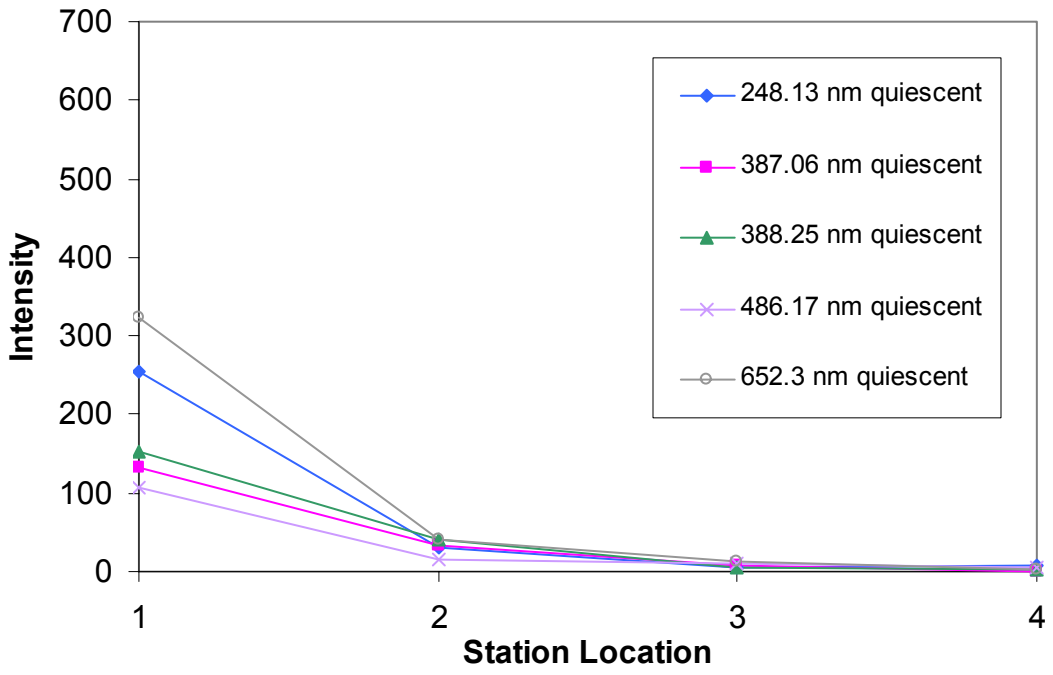

Figure B.10: Intensity Variations with Respect to Variations in Data Collection Stations of Random Peaks from Figures B.1 through B.8 from the Quiescent Environment

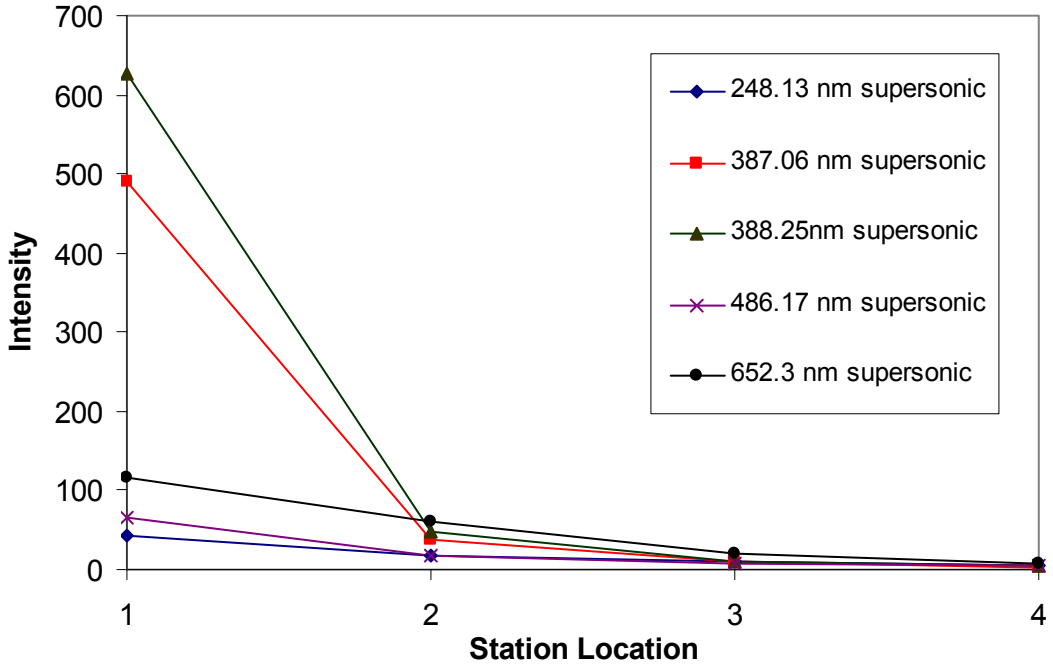

Figure B.11: Intensity Variations with Respect to Variations in Data Collection Stations of Random Peaks from Figures B.1 through B.8 from the Supersonic Environment

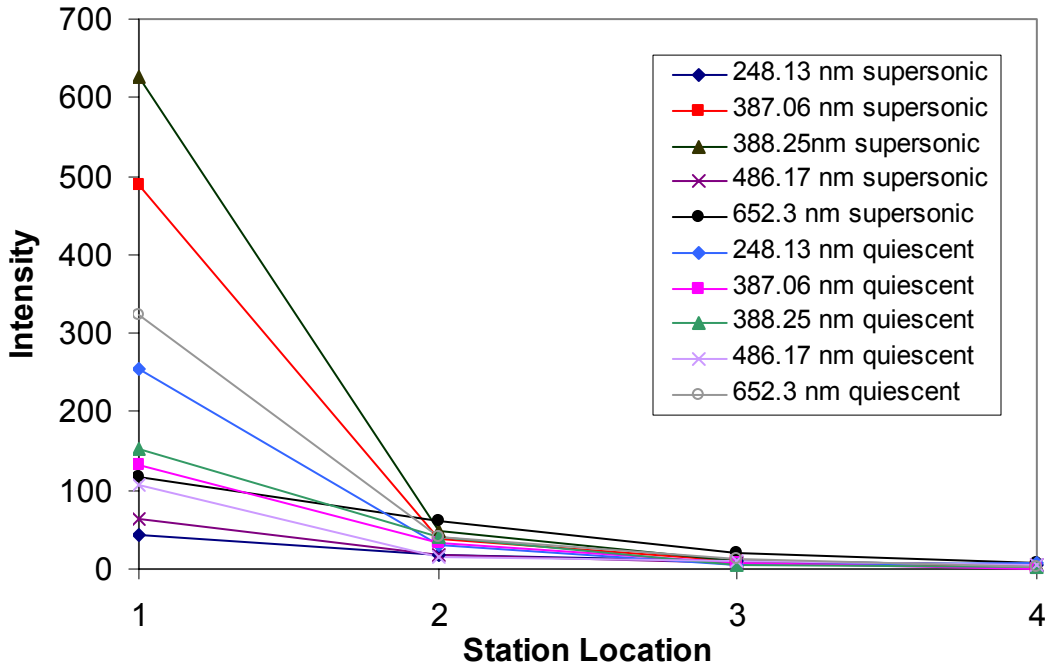

Figure B.12: Intensity Variations with Respect to Variations in Data Collection Stations of Random Peaks from Figures B.1 through B.8

Vita

Melissa Cross, daughter of Robert and Noy Cross, was born in February 1978 in Leominster, MA. She grew up in the growing suburb of Boston and eventually graduated with Honors from Leominster High School in 1996. She then attended Rochester Institute of Technology in Rochester, NY where she completed several co-ops; working for Pratt and Whitney on program implementation and technical support, as a technical writer for Emerson Electric, and as a testing technician for Carrier. She graduated, with honors and as a member of Pi Tau Sigma, with a Bachelor's degree in Mechanical Engineering and a concentration in Aerospace Engineering. After spending five years in the frigid cold and almost constant snow, she decided to continue her education and pursue a Master's degree in Mechanical Engineering in warmer weather at Virginia Tech. Upon graduation, she will begin working for Lockheed Martin as an Aeronautical Engineer in Greenville, SC.